

Supporting Information

for

O–H Stretching Frequency Red Shifts do not Correlate with the Dissociation Energies in the Dimethylether and Dimethylsulfide Complexes of Phenol Derivatives

Authors: Surjendu Bhattacharyya,[†] Sanat Ghosh,[§] and Sanjay Wategaonkar*

Department of Chemical Sciences, Tata Institute of Fundamental Research, Homi Bhabha Road,
Colaba, Mumbai 400 005, India.

Corresponding Author

*E-mail: sanwat@tifr.res.in; Phone: +91-22-2278-2259

Present Address

[†] JRM Laboratory, Kansas State University, 1228 N. 17th St. Manhattan, KS 66506-2601, USA

[§]Departamento de Química Física, Facultad de Ciencias Químicas, Universidad Complutense de Madrid,
28040 Madrid, Spain

Figures

Figure S1: Cartoon diagram describing the band origin (BO) –the lowest energy electronic transition.

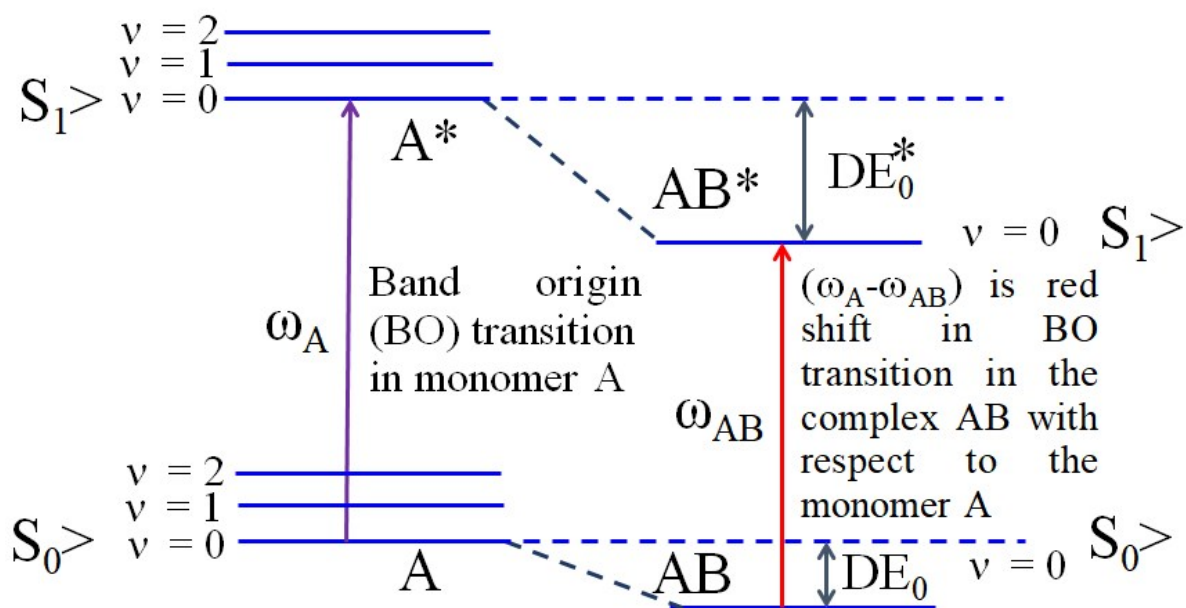
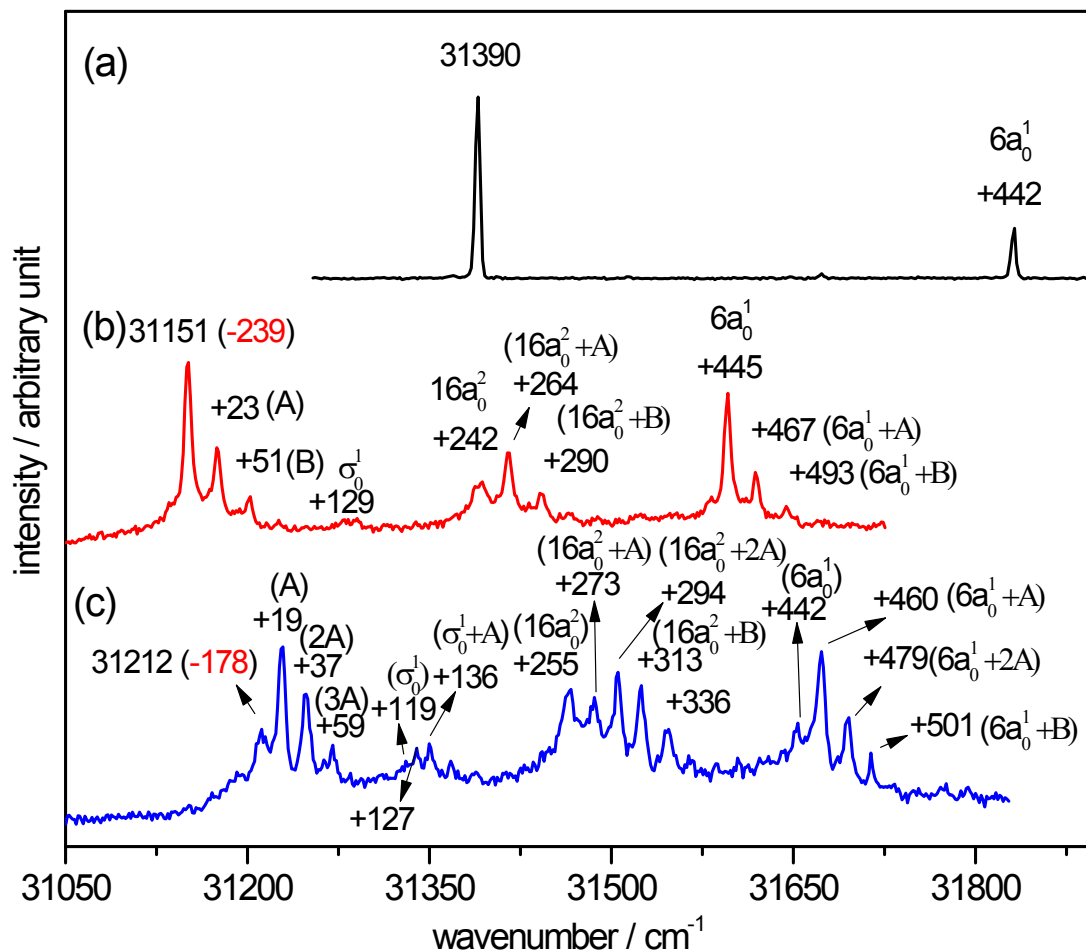


Figure S2: 1c-R2PI excitation spectra of (a) AMP, (b) AMP–Me₂O, and (c) AMP–Me₂S.

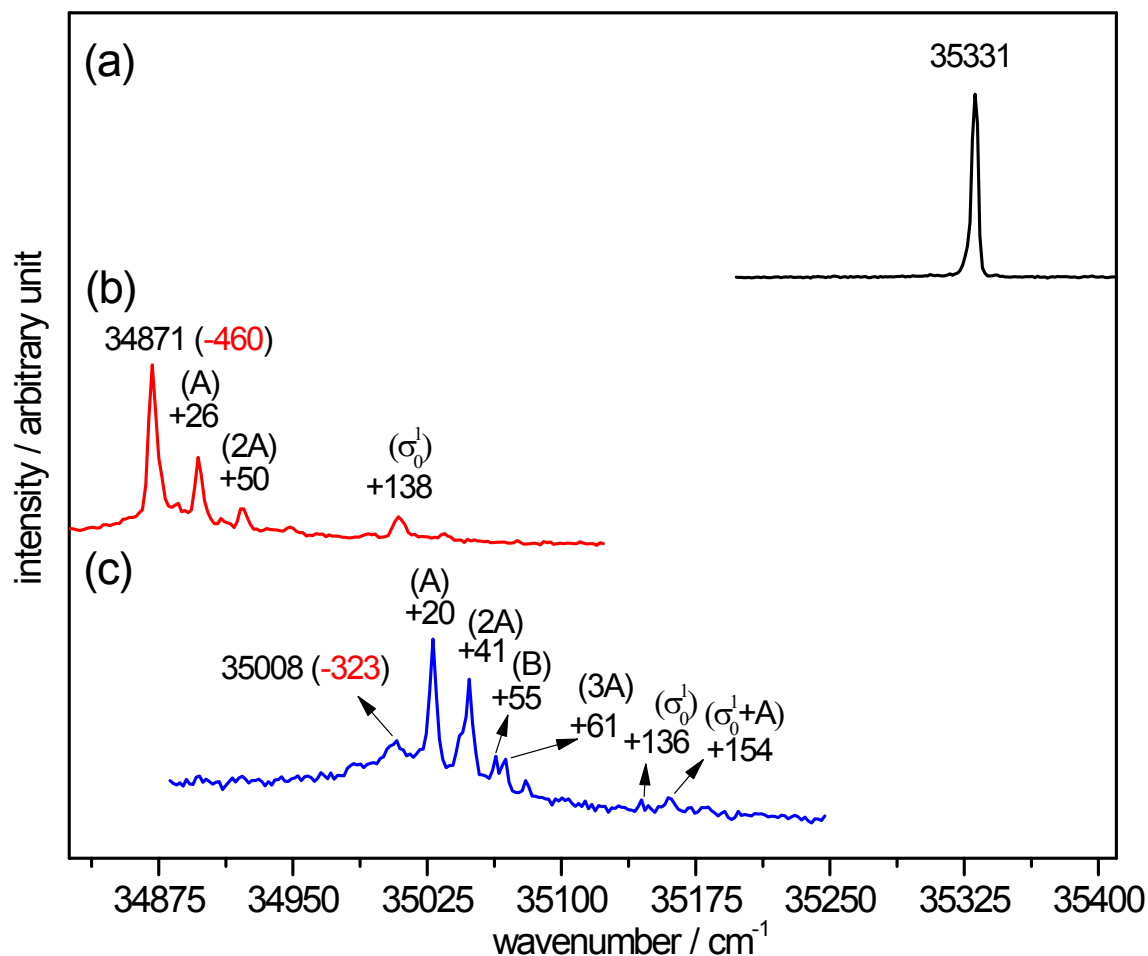


Trace a: The transition at 31832 cm⁻¹ (+442) was assigned to 6a¹.

Trace b: Couple of transitions observed near the BO at 31174 (+23; A) and 31202 cm⁻¹ (+51; B) were assigned to the low frequency intermolecular modes of the complex. The small hump near 31280 cm⁻¹ (+129) was assigned to intermolecular stretching frequency, σ^1 . Other FC active transitions found at 31393 (+242) and 31596 cm⁻¹ (+445) were ascribed to 16a² and 6a¹, respectively.

Trace c: Transition at 31212 is assigned as the BO. Very weak feature at 31331 (+119; σ^1) was assigned to intermolecular stretching mode which was accompanied by other two features at 31339 (+127), 31350 cm⁻¹ (+138; σ^1 +A). The 16a² and 6a¹ were observed at 31467 cm⁻¹ (+255) and 31654 cm⁻¹ (+442) respectively. These two intramolecular modes also occurred in combination with low energy intermolecular modes A, 2A, and B.

Figure S3: 1c-R2PI electronic excitation spectra of (a) CRL, (b) CRL–Me₂O, and (c) CRL–Me₂S.

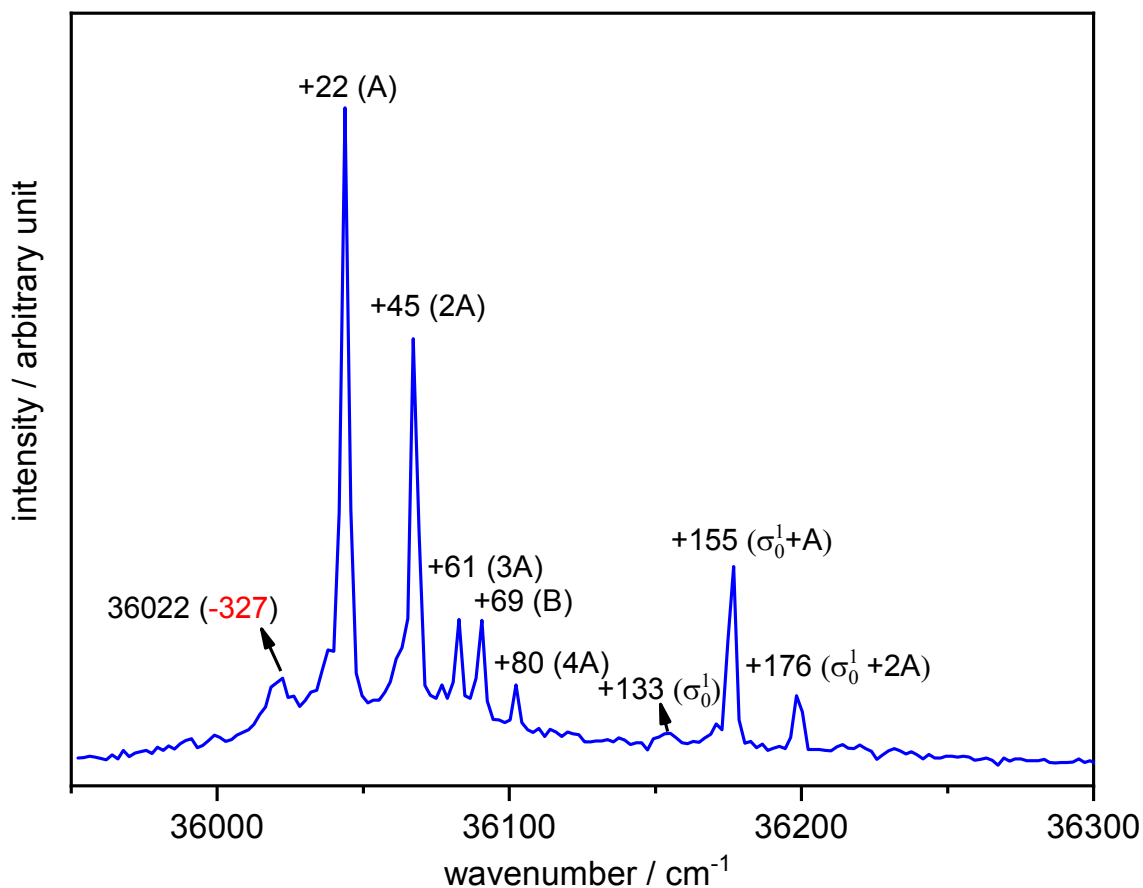


Trace a: Transition at 35331 cm⁻¹ was assigned as the BO of CRL monomer

Trace b: The BO of CRL–Me₂O complex was found at 34871 cm⁻¹. The transitions at 34897 (+26; A), and 34921 cm⁻¹ (+50, 2A) were assigned as the members of progression in 25 cm⁻¹ mode. Intermolecular stretching frequency was found at 35009 cm⁻¹ (+138; σ¹).

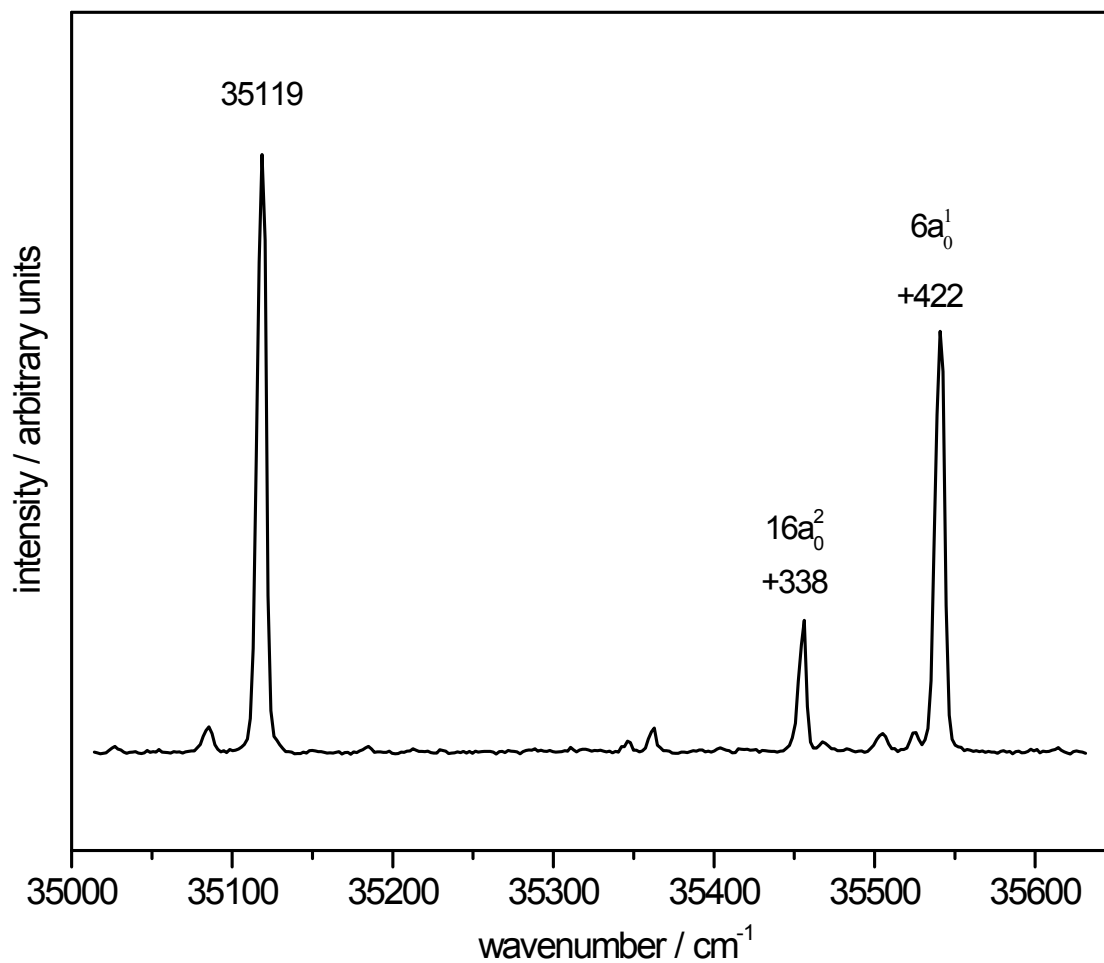
Trace c: The BO of Me₂S complex was observed at 35008 cm⁻¹. The most intense transition 35028 cm⁻¹ (+20; A) was assigned to one of the low frequency vibrational modes. Other transitions were observed at 35049 (+41; 2A), 35063 (+55; B), and 35069 cm⁻¹ (+61; 3A). The transition at 35144 cm⁻¹ (+136; σ¹) was designated as intermolecular stretching frequency; the low frequency mode A also appeared at 35162 cm⁻¹ in combination it.

Figure S4: 2c-R2PI excitation spectra of PHE–Me₂S.



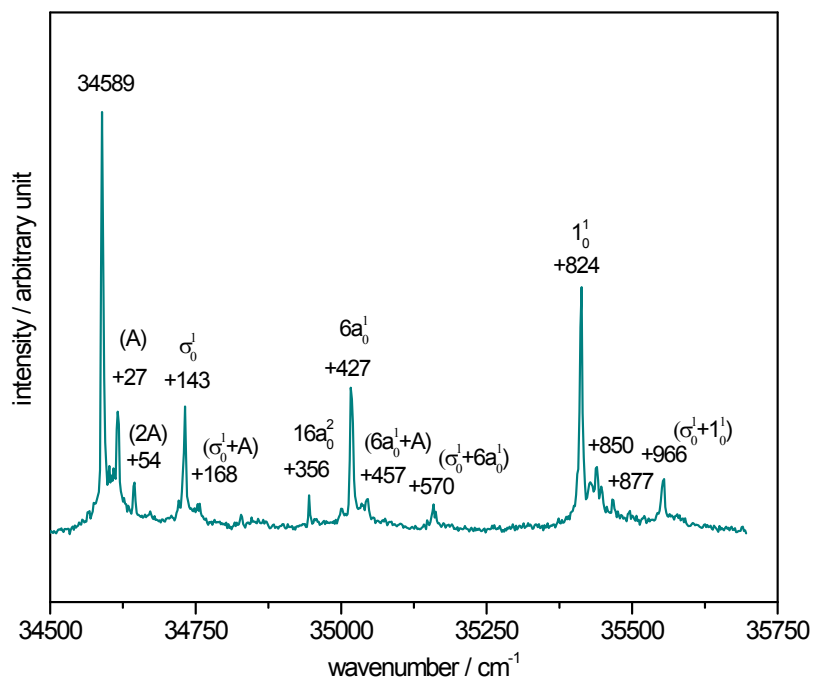
Transition at 36022 cm⁻¹ was assigned at the BO of the complex. The most intense transition at 36044 cm⁻¹ (+22) was assigned to the low frequency vibrational mode A which was accompanied by three of its progression members at 36067 (+45, 2A), 36083 (+61, 3A), and 36102 cm⁻¹ (+80, 4A), respectively. Another low frequency vibrational mode B, relatively weaker in intensity was observed at 36091 cm⁻¹ (+69, B). Intermolecular stretching frequency (σ¹) appeared at 36155 cm⁻¹ (+133, σ¹). Combination bands of σ¹ with A was identified at 36177 cm⁻¹ (+155, σ¹+A), 36198 cm⁻¹ (+176, σ¹+2A).

Figure S5: 2c-R2PI electronic excitation spectrum of *p*-Fluorophenol (FLP).



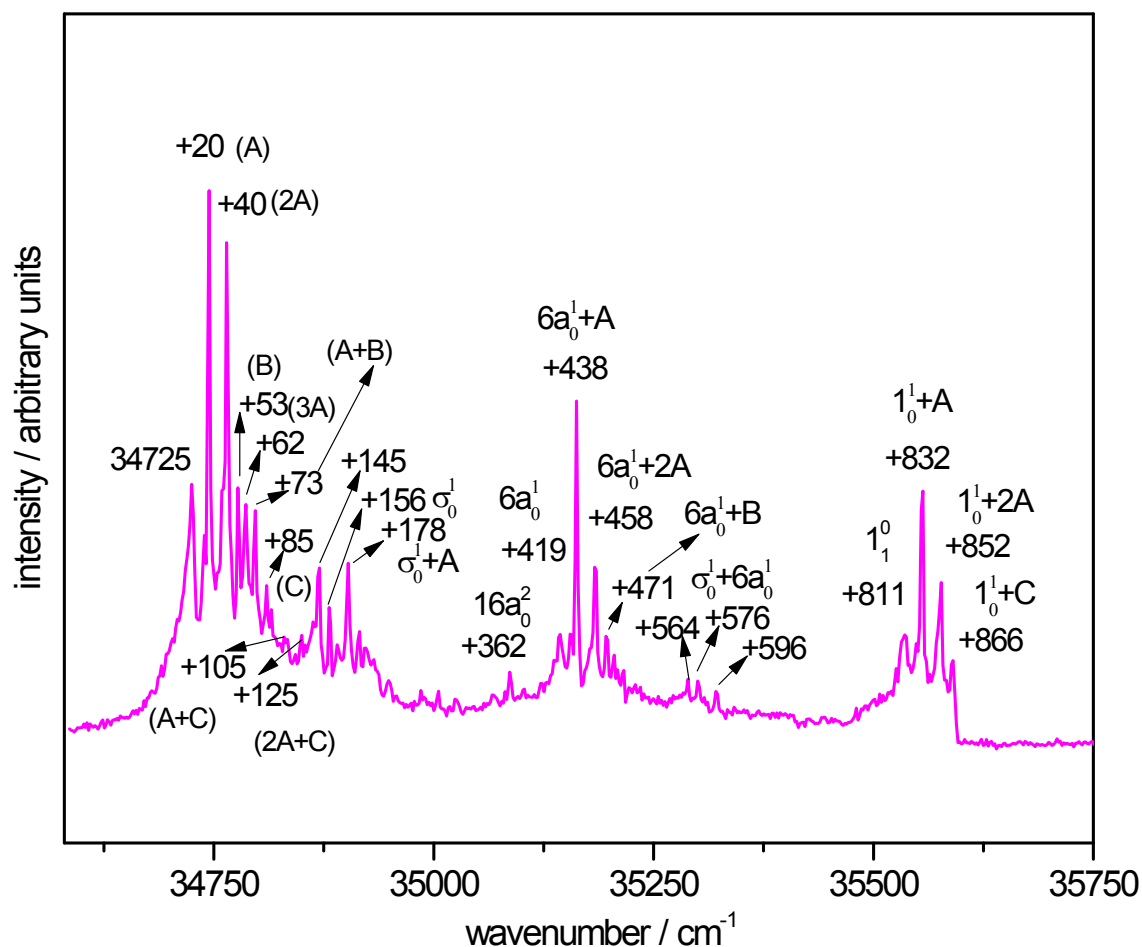
The transition at 35119 cm⁻¹ was assigned as the BO transition.^{11, 39} Transitions observed at 35457 (+338), and 35541 cm⁻¹ (+422) were assigned to 16a₀², and 6a₀¹, respectively.

Figure S6: 2c-R2PI electronic excitation spectrum of FLP–Me₂O.



The BO transition of the FLP–Me₂O complex was found at 34589 cm⁻¹. Low frequency intermolecular vibrational mode ‘A’ and its first overtone were observed at 34616 (+27) and 34643 cm⁻¹ (+54), respectively. The intermolecular stretching (σ¹) mode was found at 34732 cm⁻¹ (+143) followed by its very weak combination band with vibrational mode ‘A’ at 34757 cm⁻¹ (+168). Other transitions observed at 34945 (+356), 35016 (+427), and 35413 cm⁻¹ (+824) were assigned as the intramolecular 16a₀², 6a₀¹, and 1¹ normal modes.

Figure S7: 2c-R2PI electronic excitation spectrum of FLP–Me₂S.



The red most transition at 34725 cm⁻¹ was assigned as the BO transition. The most intense transition at 34745 cm⁻¹ (+20; A) followed by several closely spaced features at 34765 (+40; 2A), 34778 (+53; B), 34786 (+62; 3A), 34797 (+73; A+B), 34810 (+85; C), 34830 (+105; A+C), and 34850 cm⁻¹ (+125; 2A+C) were assigned to the low frequency intermolecular modes and their combinations as shown in the parentheses. The transitions at 34870 (+145), 34881 (+156, σ¹), and 34903 cm⁻¹ (+178, σ¹+A) have been identified as other intermolecular vibrations. Intramolecular vibrational modes observed at 35536 (+362), 35144 (+419), and 35536 cm⁻¹ (+811) were assigned to 16a₀², 6a₀¹, and 1¹, transitions, respectively.

Figure S8: 2c-R2PI excitation spectra of *s*-NPH–Me₂S.

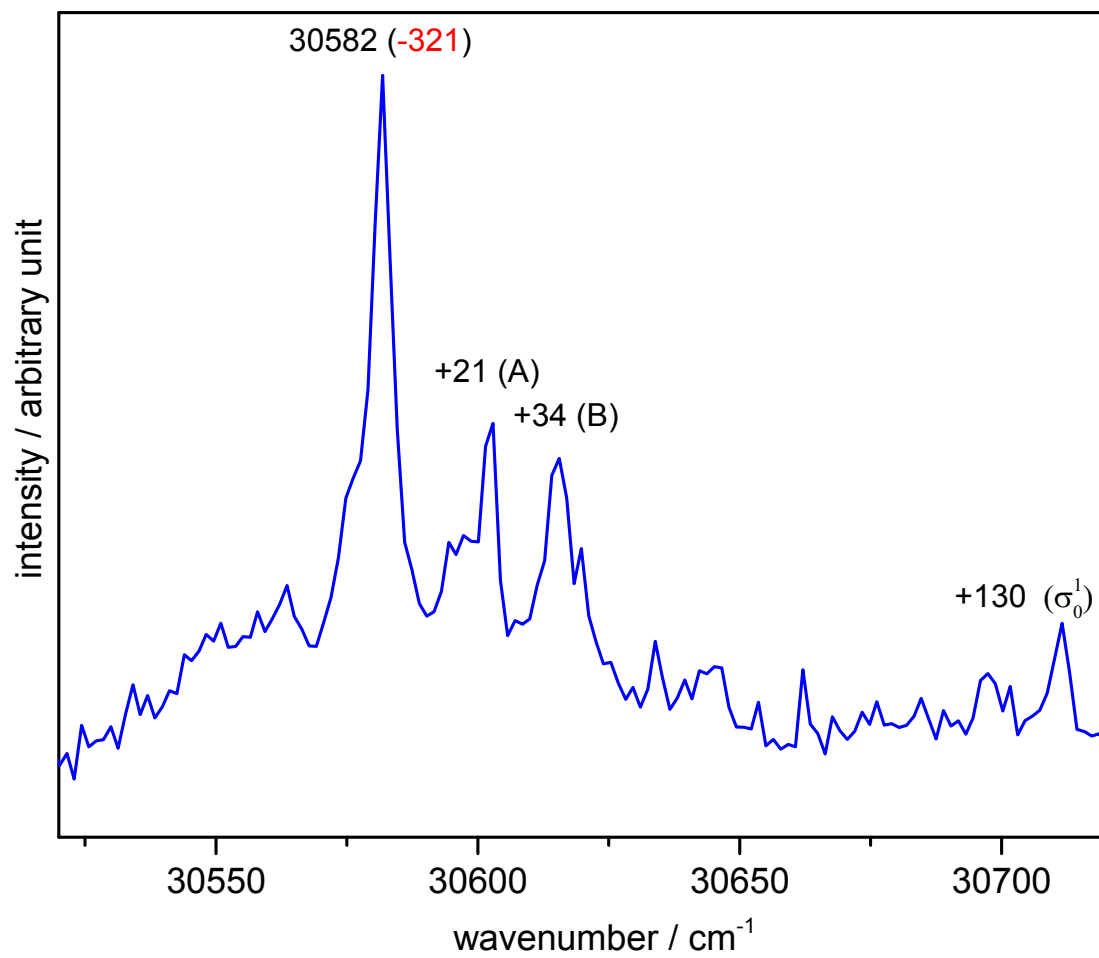
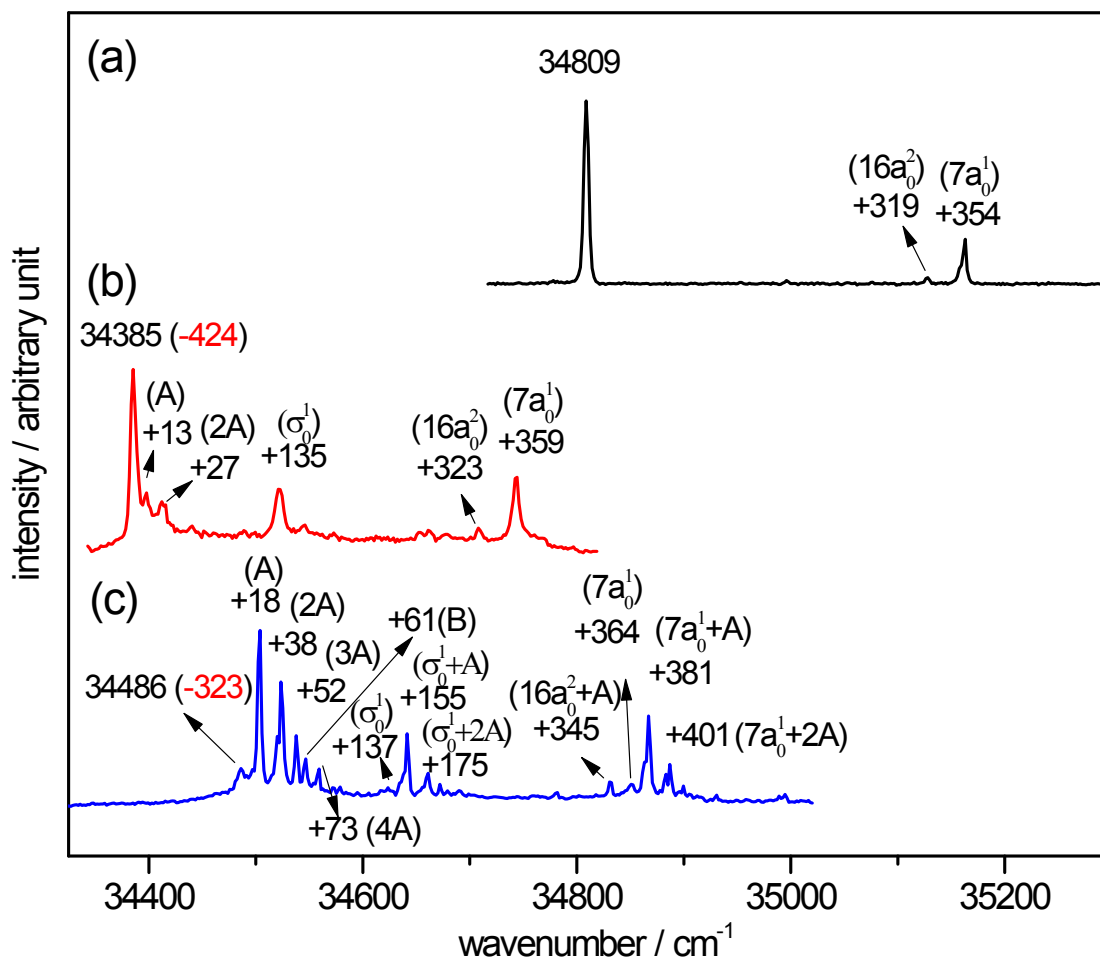


Figure S9: 1c-R2PI excitation spectra of (a) CLP, (b) CLP–Me₂O, and (c) CLP–Me₂S.



Trace a: Transition at 34809 cm⁻¹ was assigned as the BO of CLP. The 16a² and 7a¹ modes were observed at 35128 (+319), and 35163 cm⁻¹ (+354) respectively.

Trace b: The BO of CLP–Me₂O complex was at 34385 cm⁻¹. A low frequency intermolecular mode was observed at 34398 cm⁻¹ (+13; A) along with its overtone at 34412 cm⁻¹ (+27; 2A). The intermolecular stretching frequency was identified at 34521 cm⁻¹ (+136; σ¹). The transitions at 34708 (+323) and 34744 cm⁻¹ (+359) were ascribed to 16a² and 7a¹, respectively.

Trace c: The BO of Me₂S complex was observed at 34486 cm⁻¹. The most intense transition at 34504 cm⁻¹ (+18; A) was assigned as one of the low frequency vibrational modes. Other intermolecular modes and overtones were identified at 34524 (+38; 2A), 34538 (3A; +52), 34547 (+61; B) and 34559 cm⁻¹ (+73; 4A). The intermolecular stretching frequency was observed at 34623 cm⁻¹ (+137; σ¹). The transition observed at 34831 cm⁻¹ (+345) was assigned to combination band of 16a² with intermolecular vibrational mode ‘A’. Because it is considerably reasonable that owing to poor Franck Condon (FC) activity of mode 16a², it did not appear in the excitation spectra; instead the more FC active combination mode with A was observed. The transition at 34851 cm⁻¹ (+365) was ascribed to 7a¹.

Figure S10: IR-UV hole burning spectra of AMP–Me₂O in R2PI mode.

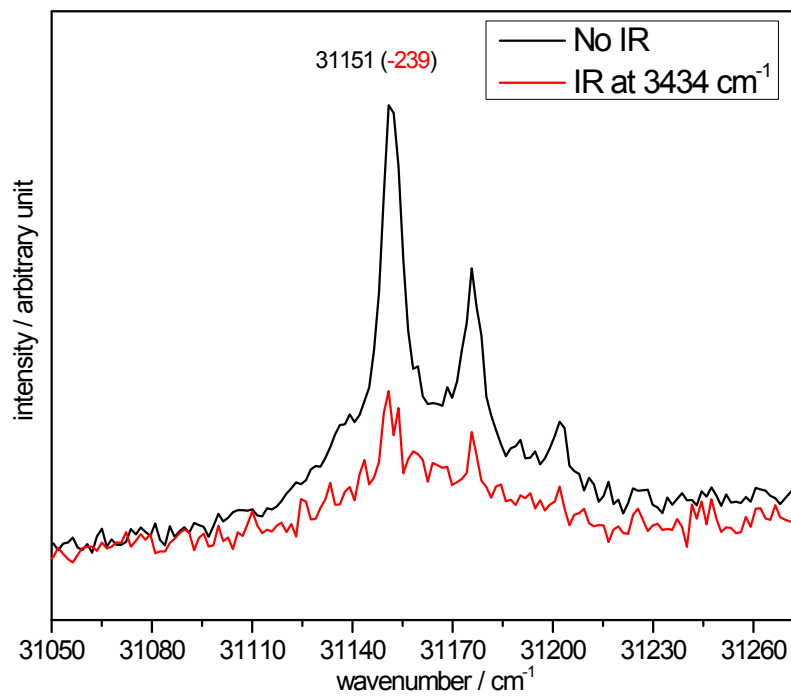


Figure S11: IR-UV hole burning spectra of AMP–Me₂S in R2PI mode.

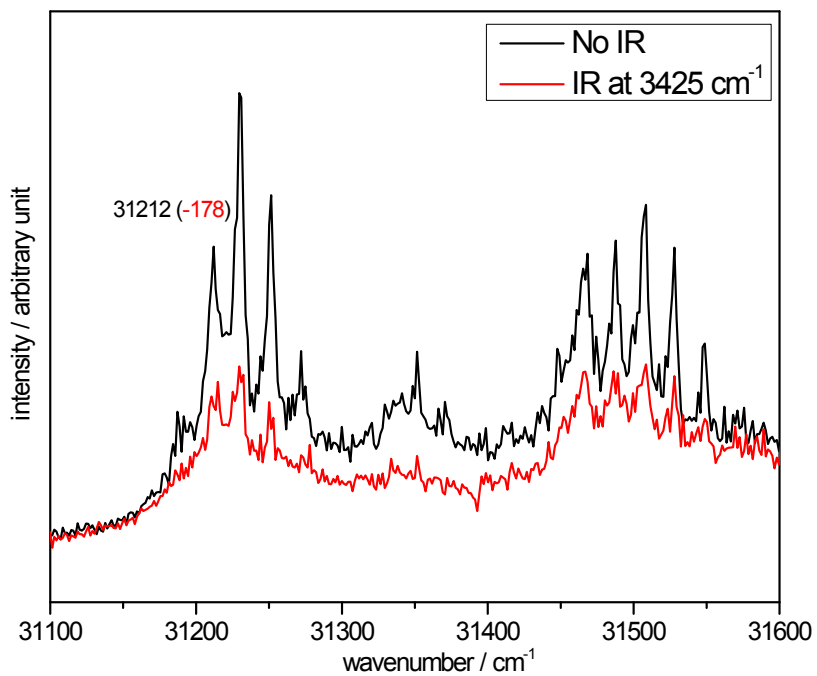


Figure S12: FDIR spectra of CRL–Me₂O by while the excitation laser was tuned to (a) 34897 cm⁻¹ and (b) 34923 cm⁻¹.

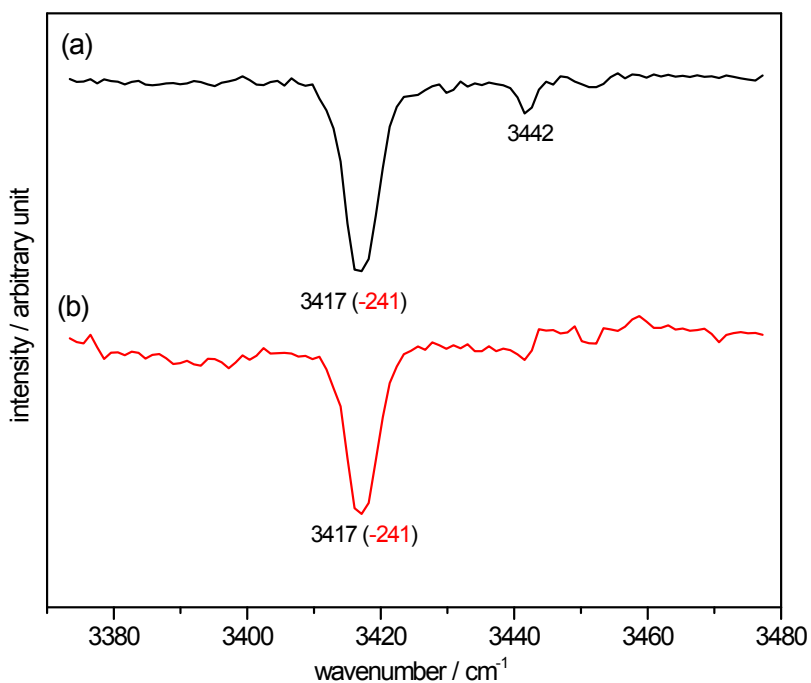


Figure S13: (a) FDIR spectra of CRL–Me₂S by while the excitation laser was tuned to 35049 cm⁻¹ and (b) RIDIR spectra of CRL–Me₂S by while the excitation laser was tuned to 35028 cm⁻¹.

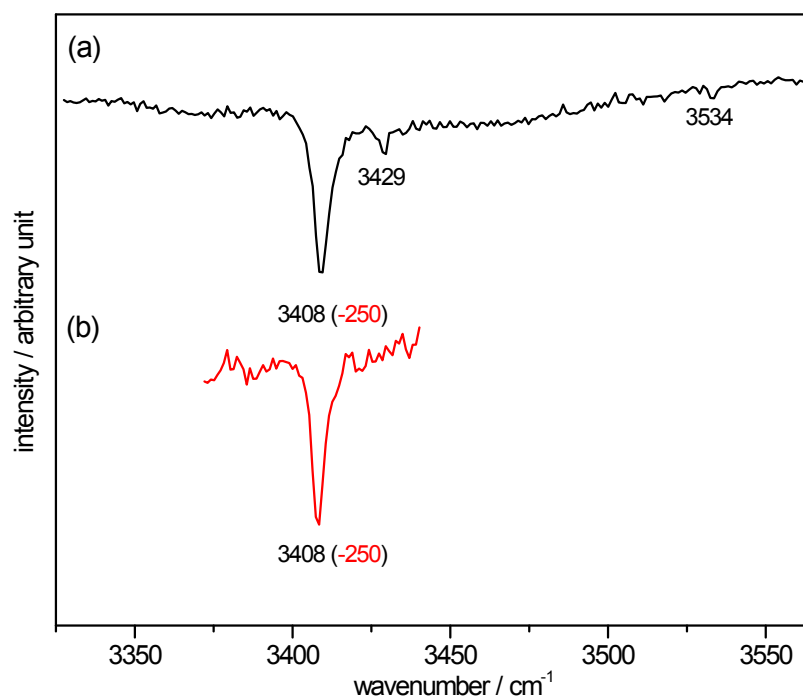


Figure S14: IR-UV hole burning spectra of CRL–Me₂O in R2PI mode.

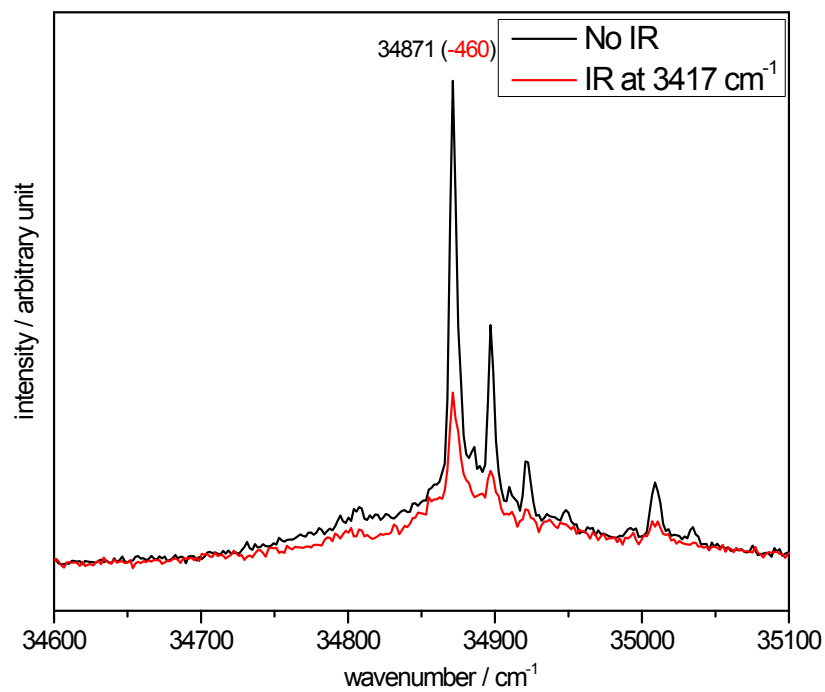


Figure 15: IR-UV hole burning spectra of CRL–Me₂S in R2PI mode.

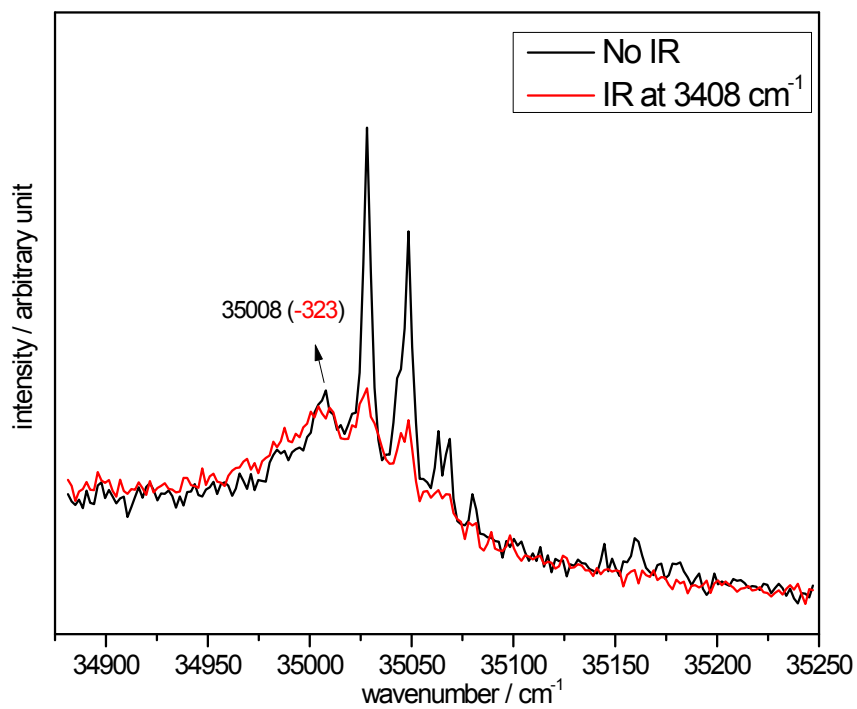


Figure S16: IR-UV hole burning spectrum of FLP-Me₂O.

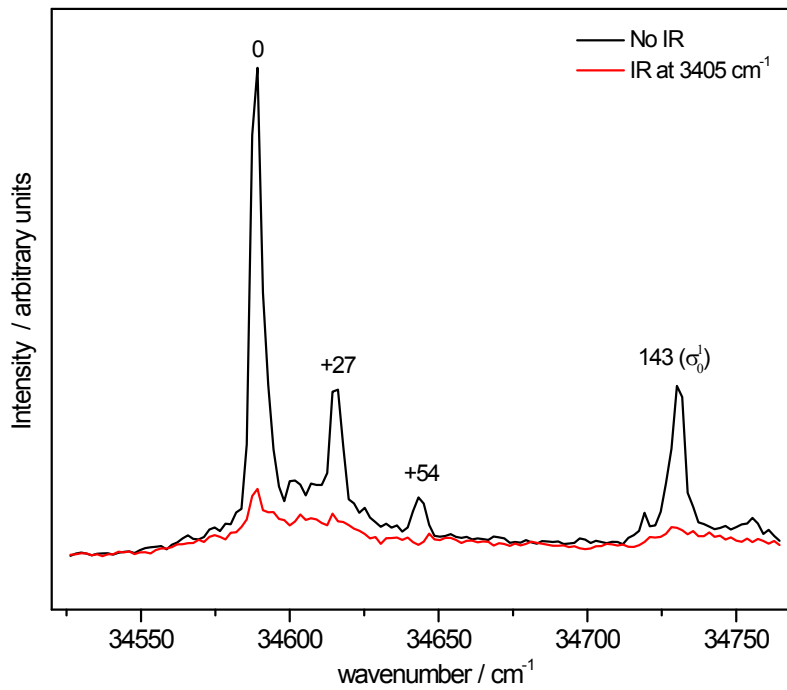


Figure S17: IR-UV hole burning spectrum of FLP-Me₂S.

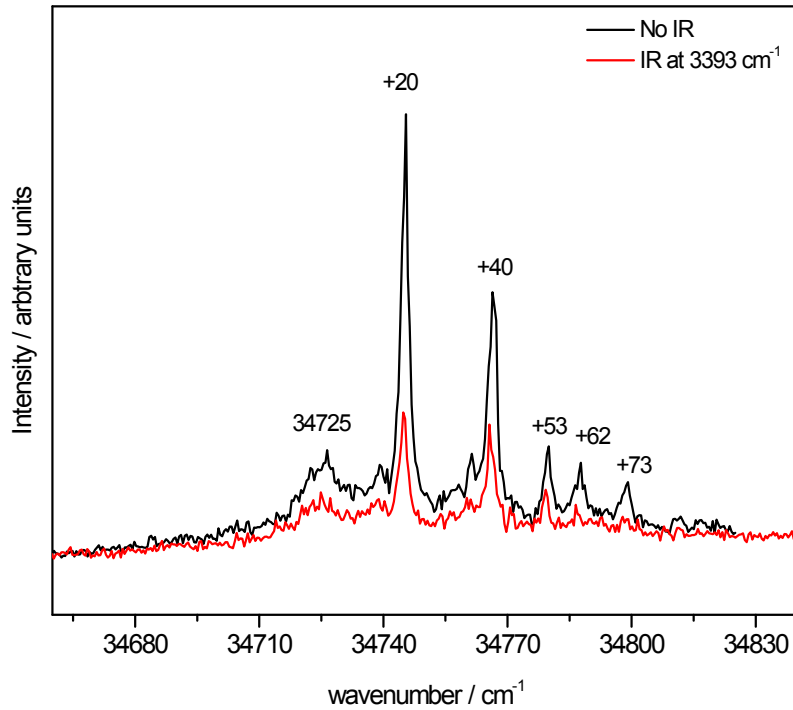


Figure S18: RIDIR spectra of FLP–Me₂S recorded by probing (a) 34725 cm⁻¹, (b) 34745 cm⁻¹, and (c) 34765 cm⁻¹ transitions.

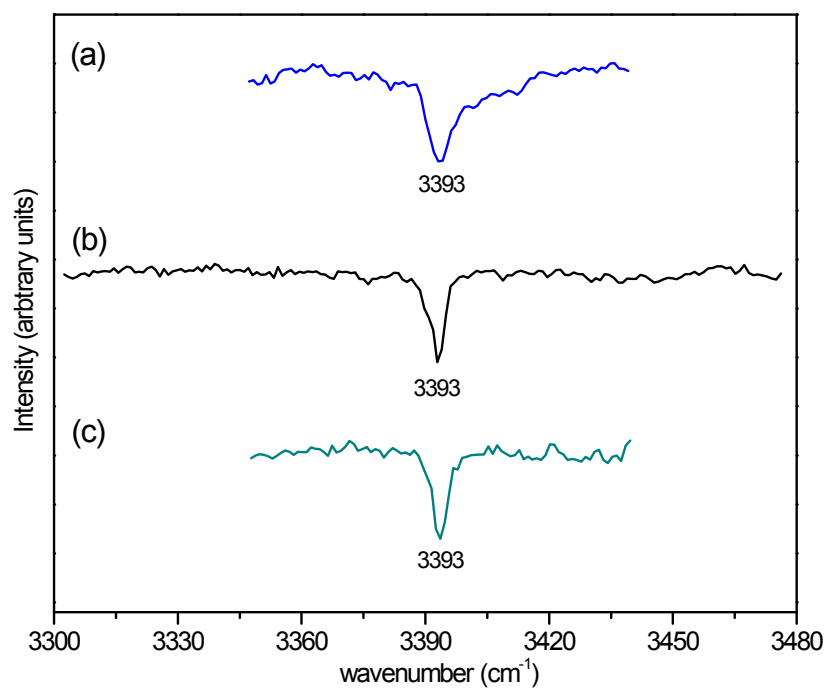


Figure S19: RIDIR spectra of CLP–Me₂O by while the excitation laser was tuned to (a) 34385 cm⁻¹, (b) 34398 cm⁻¹, (c) 34412 cm⁻¹, and (d) 34520 cm⁻¹.

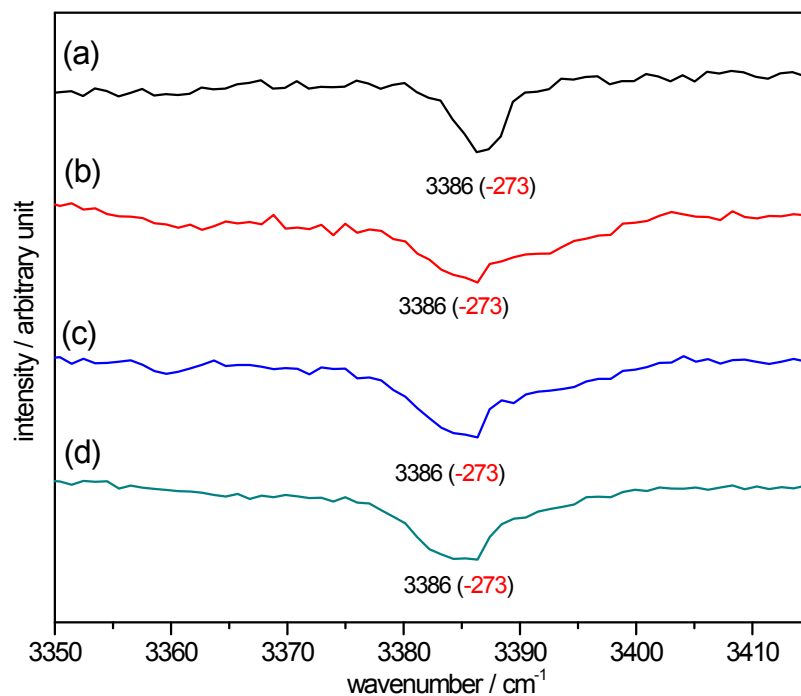


Figure S20: IR-UV hole burning spectra of CLP–Me₂O in R2PI mode.

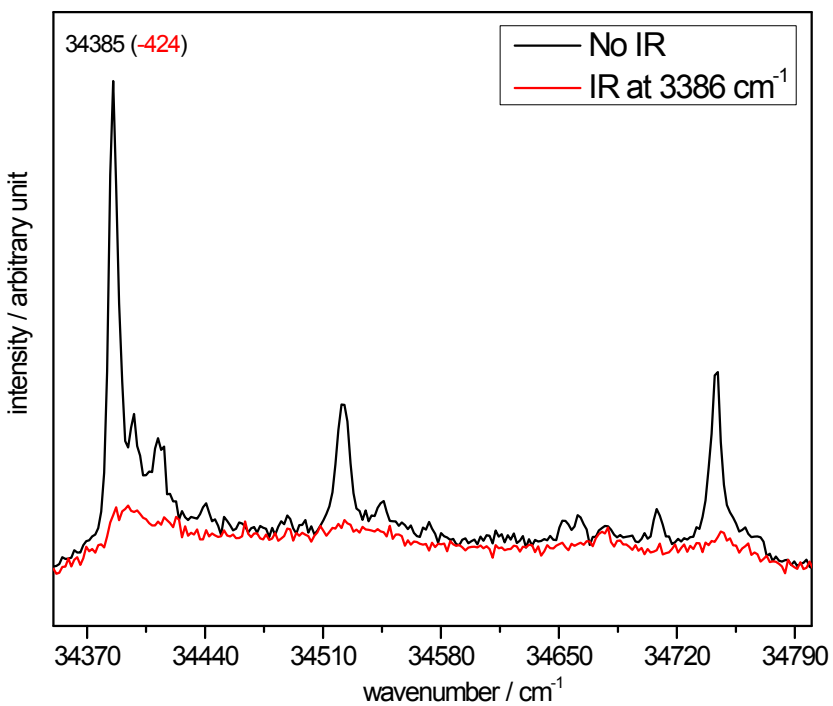


Figure S21: RIDIR spectra of CLP–Me₂S by while the excitation laser was tuned to (a) 34504 cm⁻¹, (b) 34523 cm⁻¹, and (c) 34538 cm⁻¹.

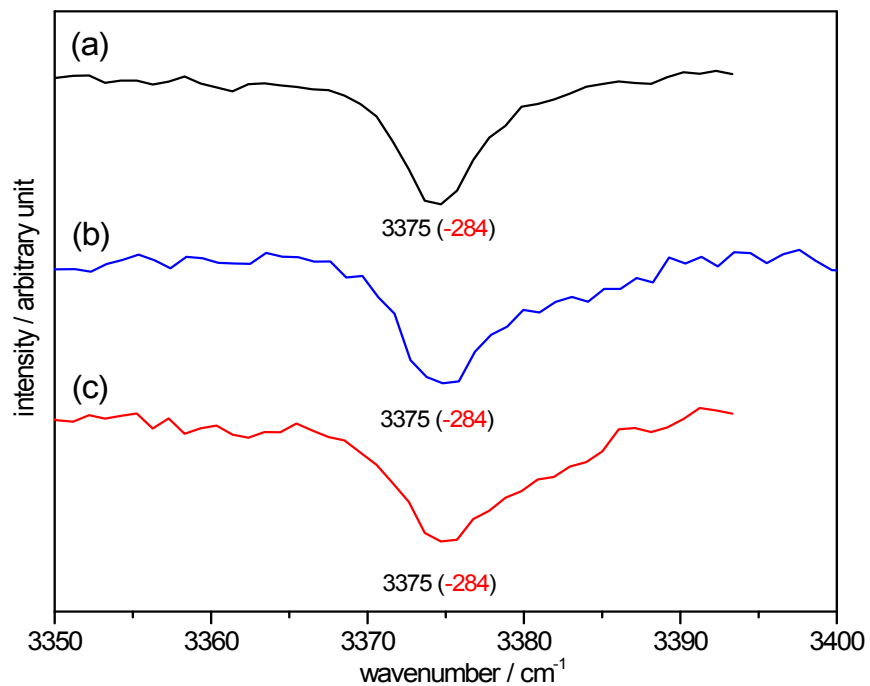


Figure S22: IR-UV hole burning spectra of CLP–Me₂S in R2PI mode.

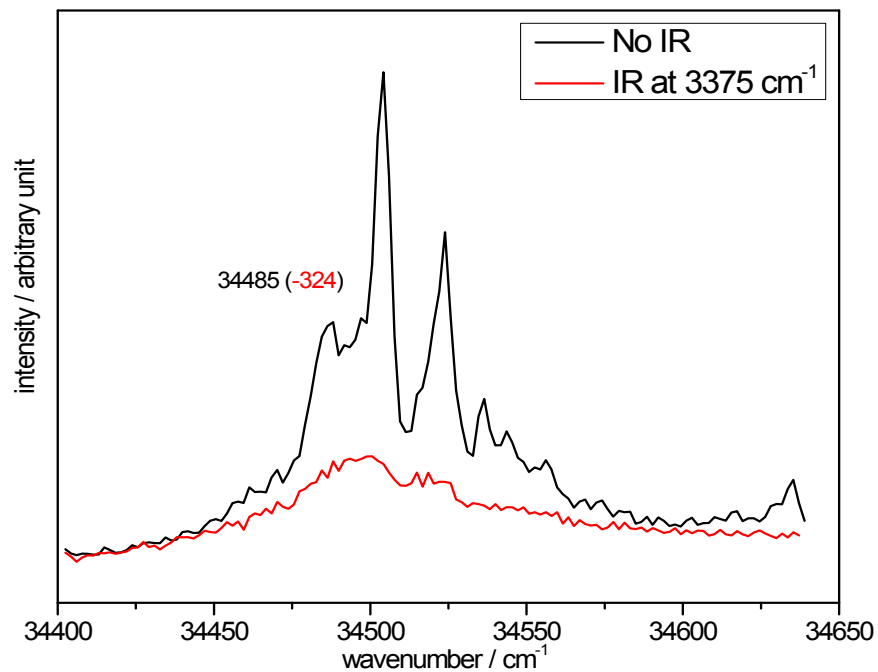
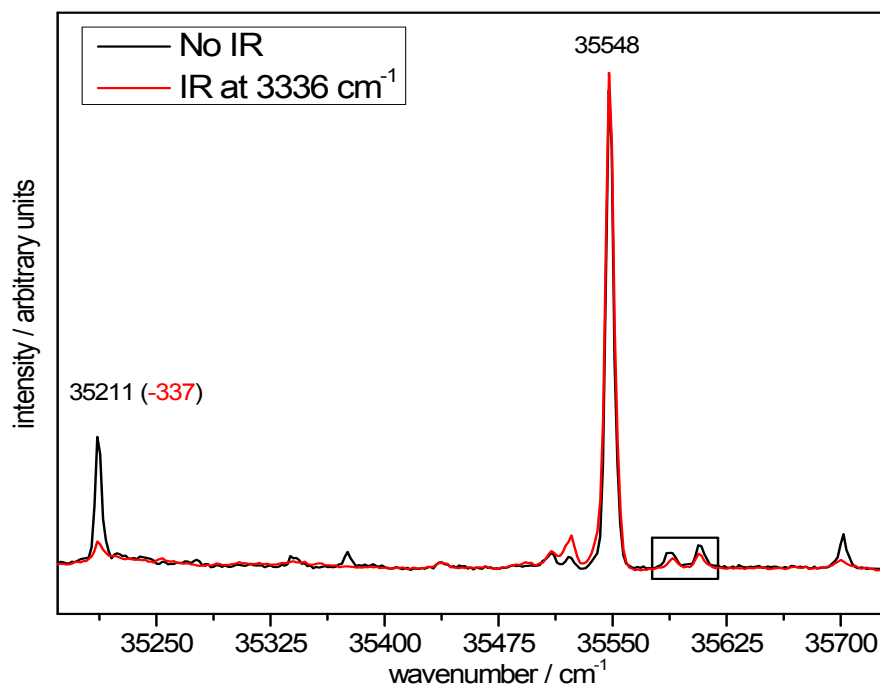
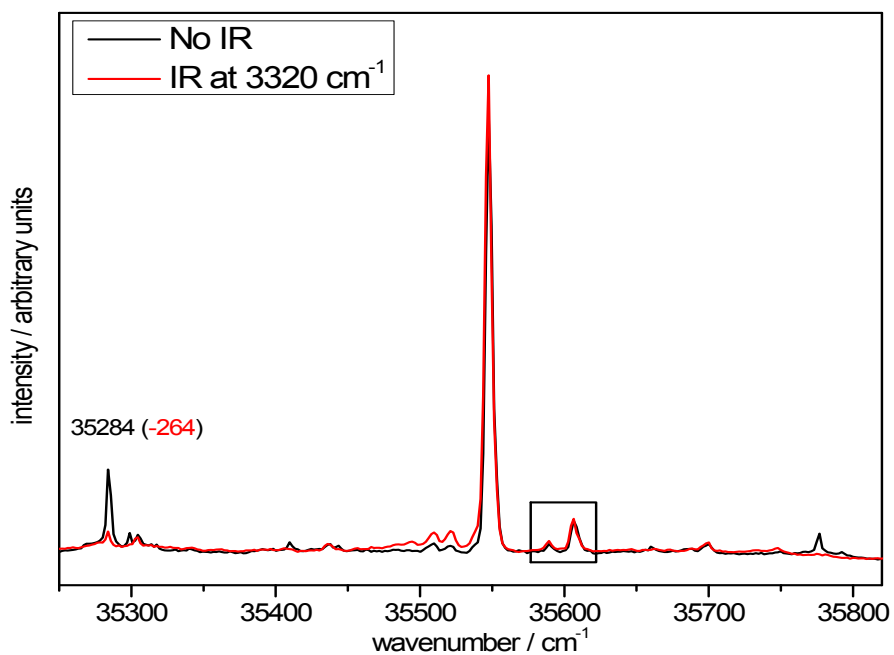


Figure S23: IR-UV hole burning spectra of CNP–Me₂O in LIF mode. Transitions within the black rectangles are the 7a¹ mode of CLP monomer which was present as a trace amount inside the chamber.



In trace o, the strong transition at 35548 cm⁻¹ was ascribed to BO of CNP. In the trace p of **Figure 1**, an additional feature appeared at 35211 cm⁻¹ when ~0.25% premix of Me₂O in He was sent as buffer gas. This peak was assigned to BO of CNP–Me₂O which was 337 cm⁻¹ red shifted with respect to monomer's BO.

Figure S24: IR-UV hole burning spectra of CNP–Me₂S in LIF mode. Transitions within the black boxed area due to the trace quantities of sample (CLP) used earlier and are not real features of that complex.



As shown in trace q of **Figure 1**, using ~0.25% premix of Me₂S in He as buffer gas a transition was observed at 35284. The BO of CNP–Me₂S was assigned as 35284 cm⁻¹ which was 264 cm⁻¹ red shifted with respect to the monomer BO.

Figure S25: The optimized structure of FLP–Me₂S at cp-MP2/aug-cc-pVDZ level. The atom number 23 is the dummy (D) one such that the line A₁₄D₂₃ bisects the $\angle C_{19}A_{14}C_{15}$ (A=O/S); $\theta = \angle O_7H_{13}A_{14}$; $\psi = \angle H_{13}A_{14}D_{23}$; Φ = Dihedral angle formed by C₄C₁O₇H₁₃; Φ' = Dihedral angle formed by C₄C₁O₇A₁₄.

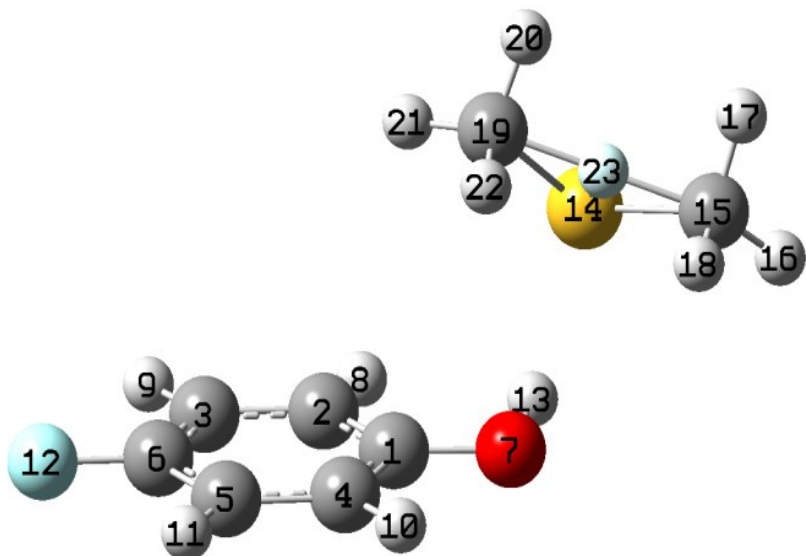


Figure S26: Molecular graph of AMP–Me₂O generated from the wave function obtained by QTAIM analysis at MP2/aug-cc-pVDZ level. Red-dots are (3,-1) bond critical points.

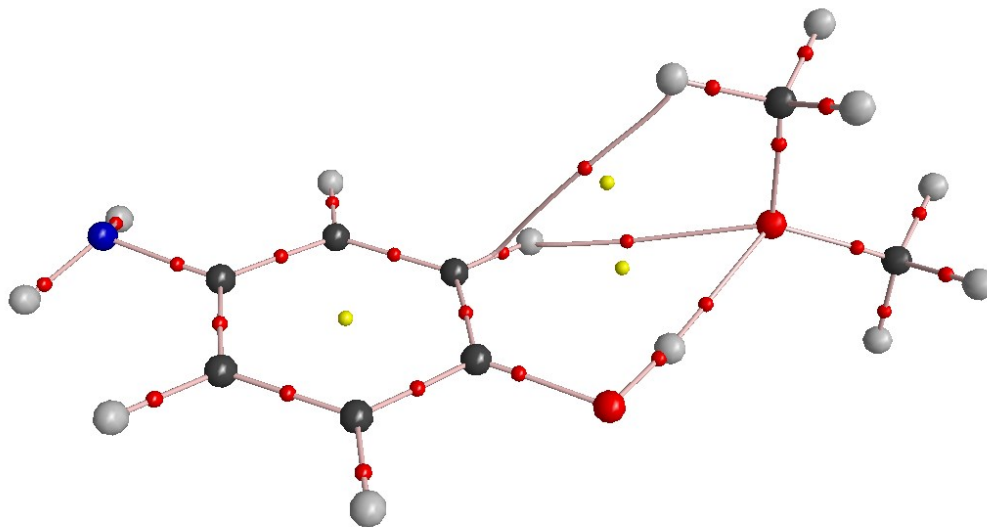


Figure S27: Molecular graph of AMP–Me₂S generated from the wave function obtained by QTAIM analysis at MP2/aug-cc-pVDZ level. Red-dots are (3,-1) bond critical points.

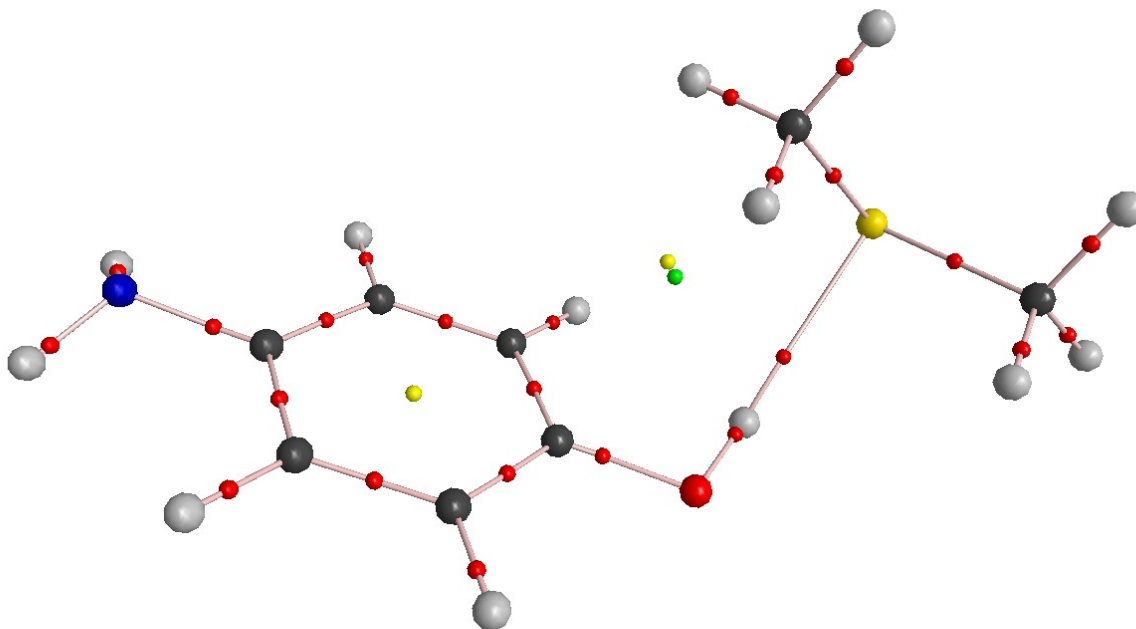


Figure S28: Molecular graph of CRL–Me₂O generated from the wave function obtained by QTAIM analysis at MP2/aug-cc-pVDZ level. Red-dots are (3,-1) bond critical points.

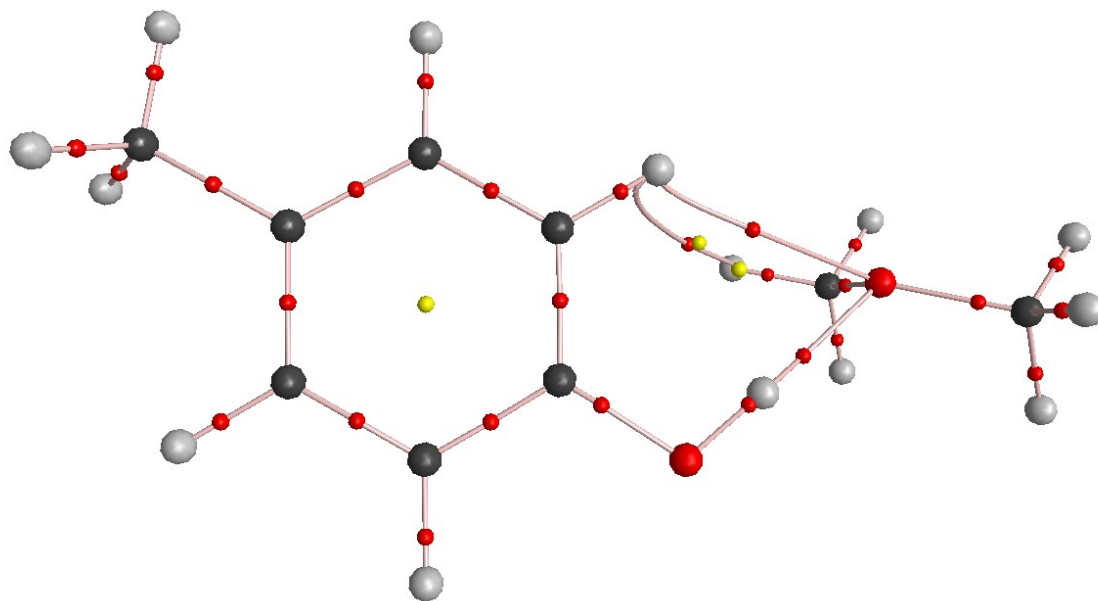


Figure S29: Molecular graph of CRL–Me₂S generated from the wave function obtained by QTAIM analysis at MP2/aug-cc-pVDZ level. Red-dots are (3,-1) bond critical points.

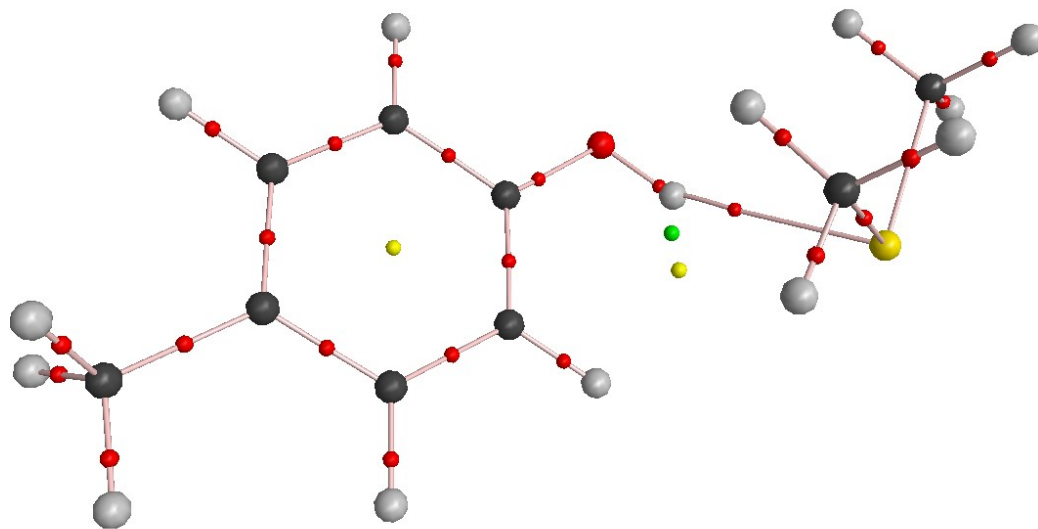


Figure S30: Molecular graph of PHE–Me₂O generated from the wave function obtained by QTAIM analysis at MP2/aug-cc-pVDZ level. Red-dots are (3,-1) bond critical points.

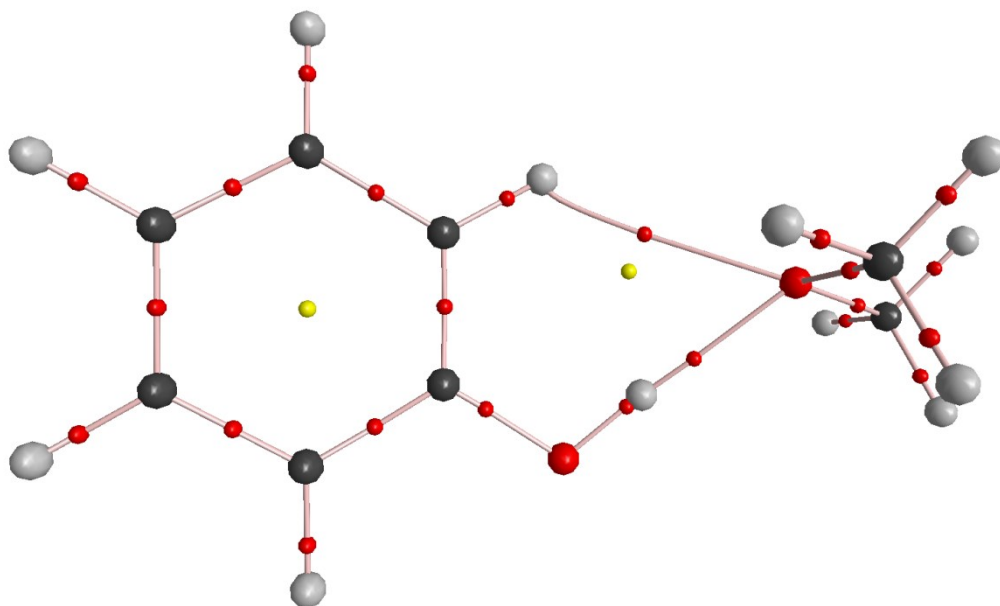


Figure S31: Molecular graph of PHE–Me₂S generated from the wave function obtained by QTAIM analysis at MP2/aug-cc-pVDZ level. Red-dots are (3,-1) bond critical points.

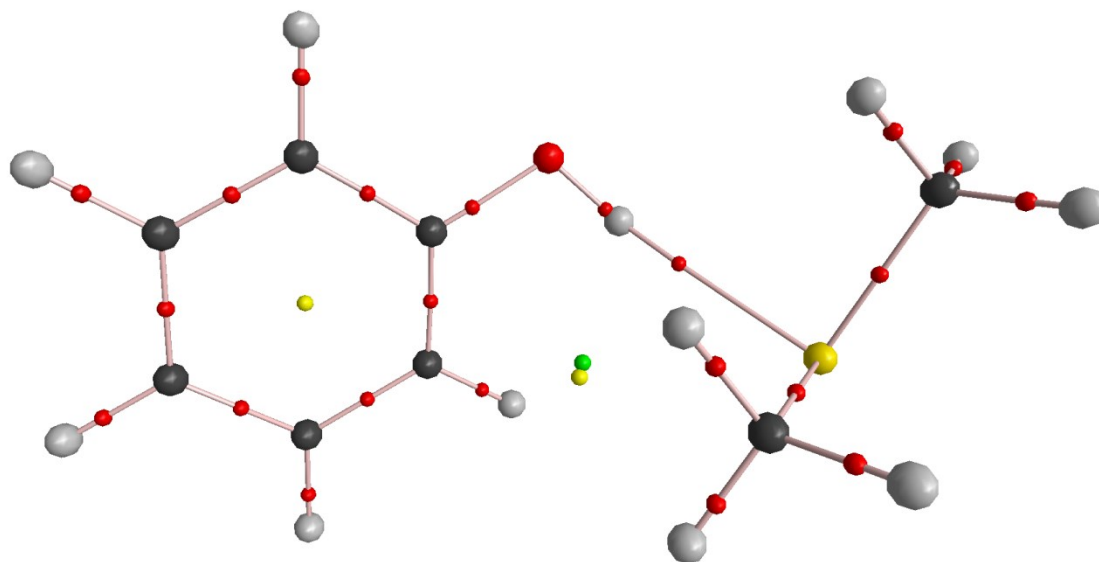


Figure S32: Molecular graph of FLP–Me₂O generated from the wave function obtained by QTAIM analysis at MP2/aug-cc-pVDZ level. Red-dots are (3,-1) bond critical points.

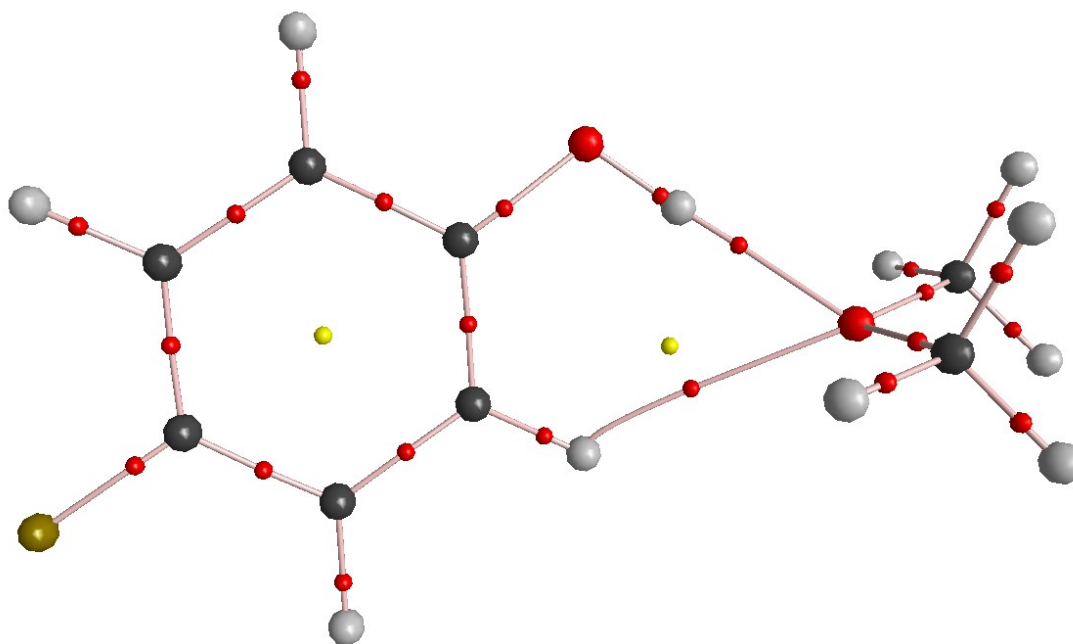


Figure S33: Molecular graph of FLP–Me₂S generated from the wave function obtained by QTAIM analysis at MP2/aug-cc-pVDZ level. Red-dots are (3,-1) bond critical points.

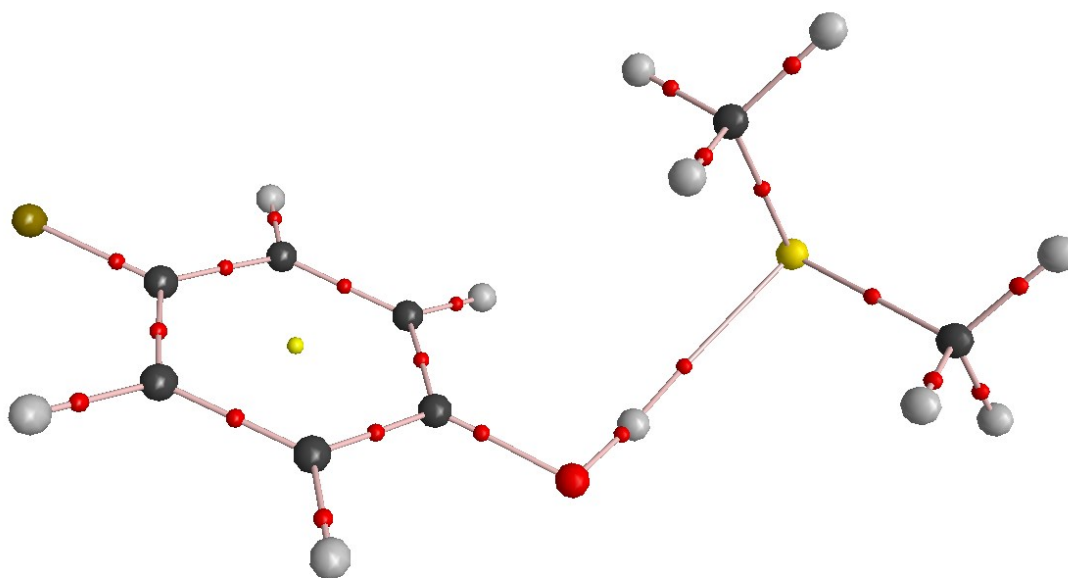


Figure S34: Molecular graph of *s*-NPH–Me₂O generated from the wave function obtained by QTAIM analysis at MP2/aug-cc-pVDZ level. Red-dots are (3,-1) bond critical points.

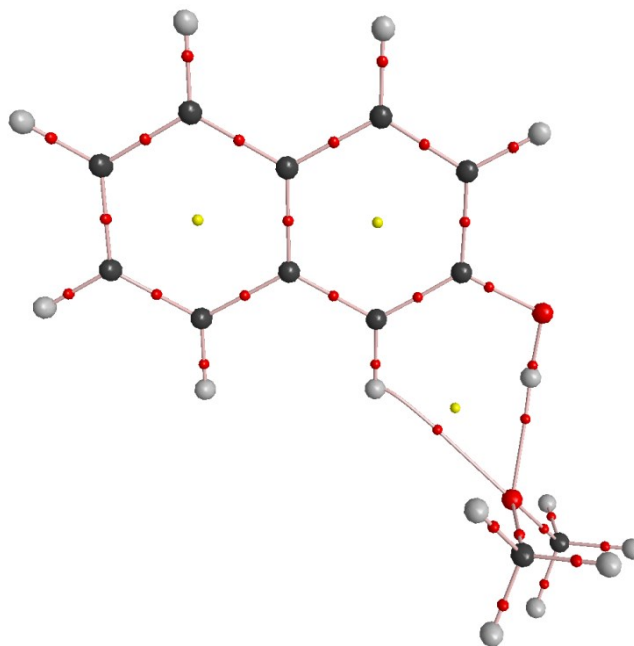


Figure S35: Molecular graph of *s*-NPH–Me₂S generated from the wave function obtained by QTAIM analysis at MP2/aug-cc-pVDZ level. Red-dots are (3,-1) bond critical points.

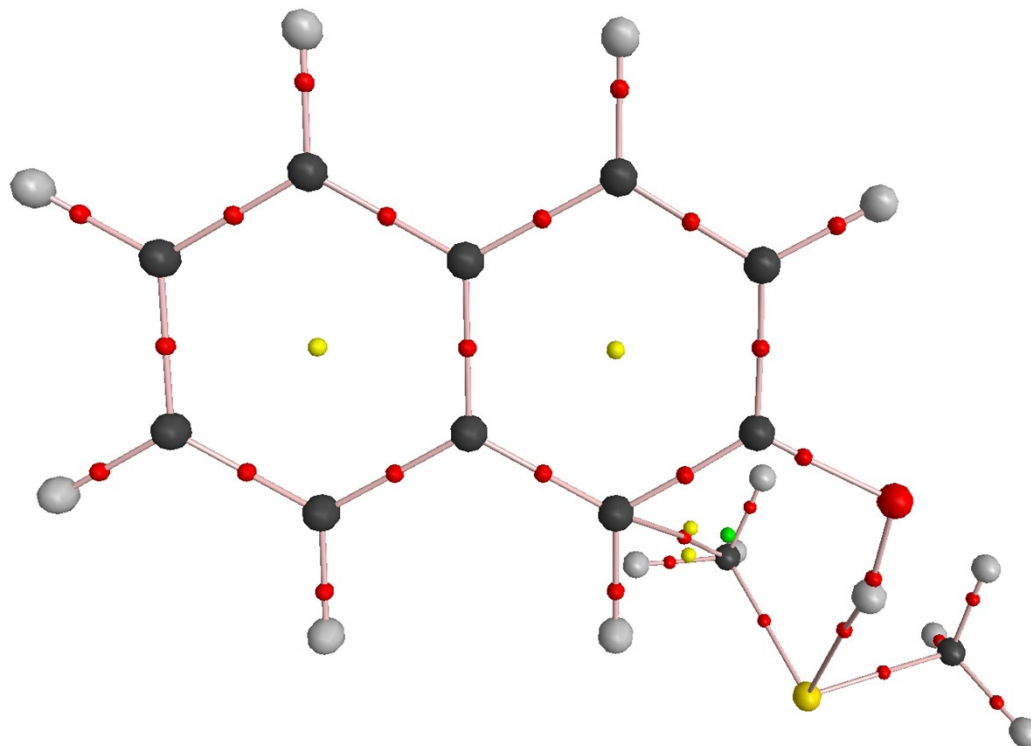


Figure S36: Molecular graph of CLP–Me₂O generated from the wave function obtained by QTAIM analysis at MP2/aug-cc-pVDZ level. Red-dots are (3,-1) bond critical points.

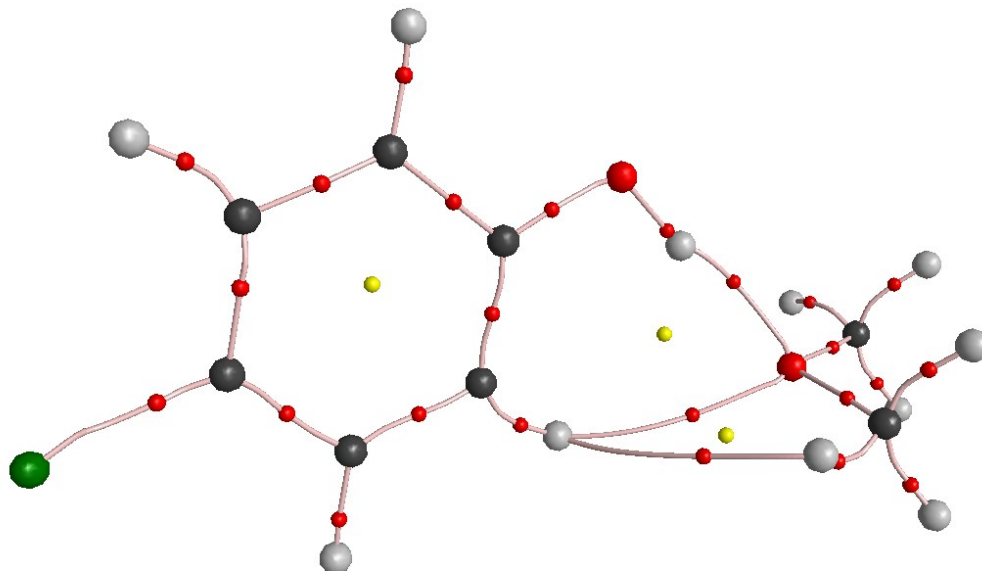


Figure S37: Molecular graph of CLP–Me₂S generated from the wave function obtained by QTAIM analysis at MP2/aug-cc-pVDZ level. Red-dots are (3,-1) bond critical points.

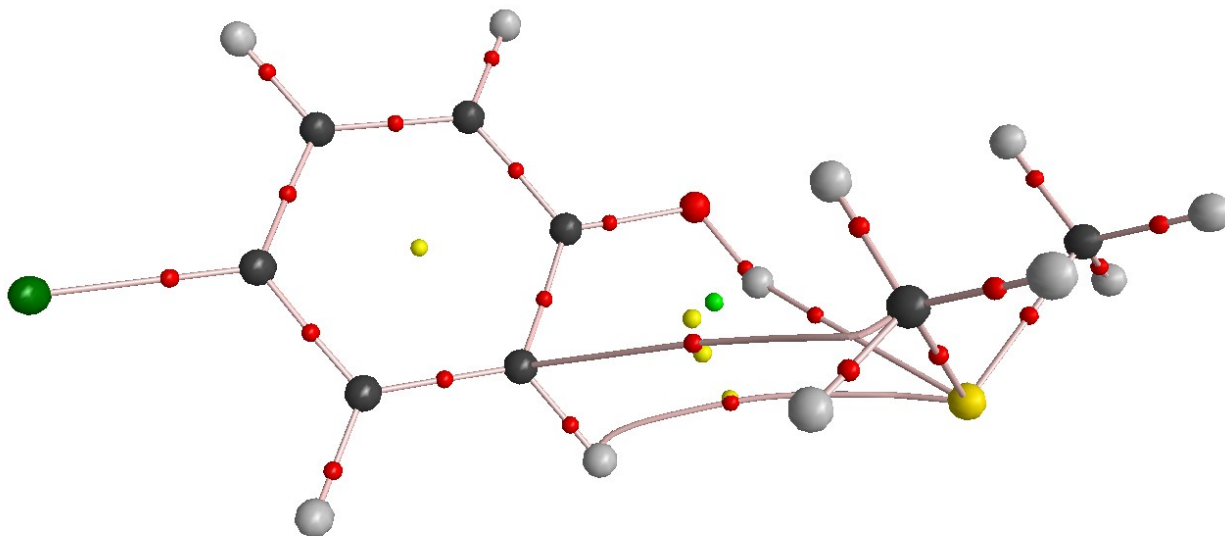


Figure S38: Molecular graph of CNP–Me₂O generated from the wave function obtained by QTAIM analysis at MP2/aug-cc-pVDZ level. Red-dots are (3,-1) bond critical points.

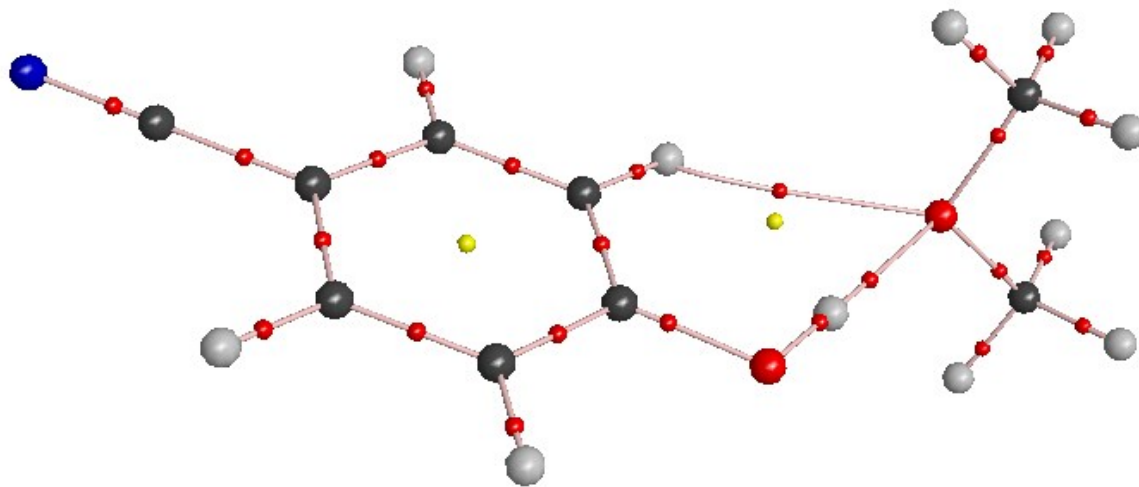


Figure S39: Molecular graph of CNP–Me₂S generated from the wave function obtained by QTAIM analysis at MP2/aug-cc-pVDZ level. Red-dots are (3,-1) bond critical points.

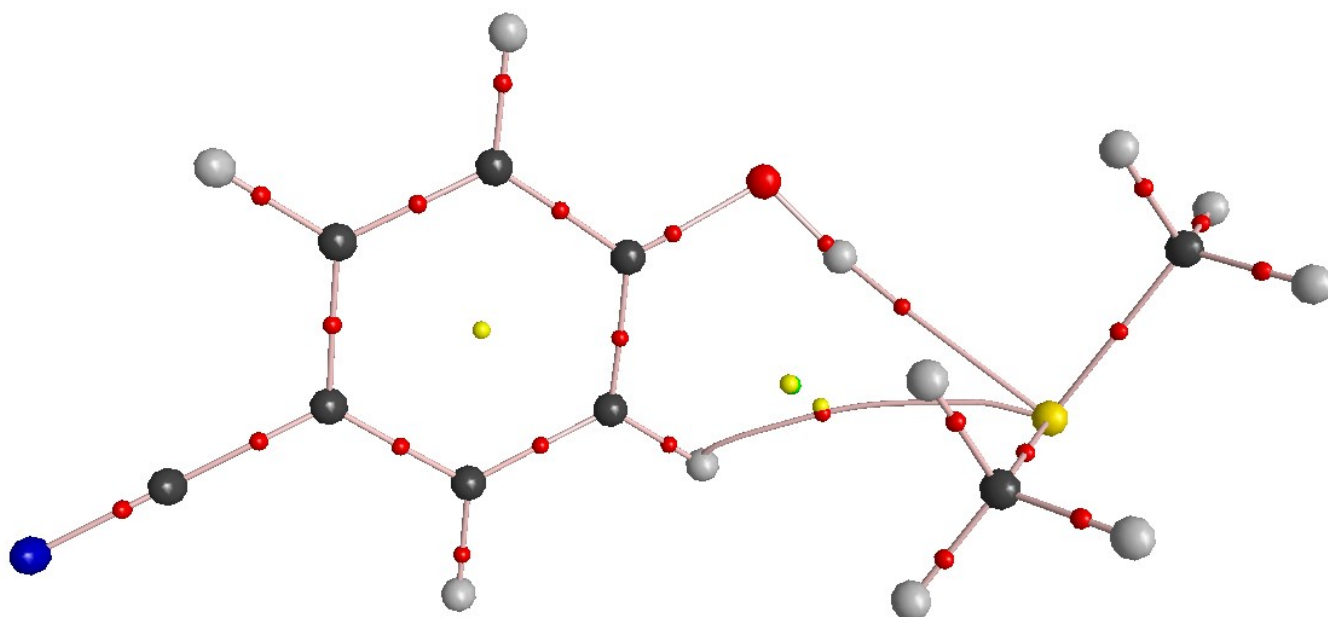


Figure S40: 2D NCI plots. The reduced density gradient (S) vs. the electron density multiplied by the sign of the second Hessian eigenvalue (λ_2). (a) AMP–Me₂O, (b) CRL–Me₂O, (c) PHE–Me₂O, (d) FLP–Me₂O, (e) *s*-NPH–Me₂O, (f) CLP–Me₂O, (g) CNP–Me₂O, (h) AMP–Me₂S, (i) CRL–Me₂S, (j) PHE–Me₂S, (k) FLP–Me₂S, (l) *s*-NPH–Me₂S, (m) CLP–Me₂S, and (n) CNP–Me₂S. The data was obtained by evaluating cp-MP2/aug-cc-pVDZ density. The O–H•••A (A=O/ S) bond critical points are indicated by the black dotted circles.

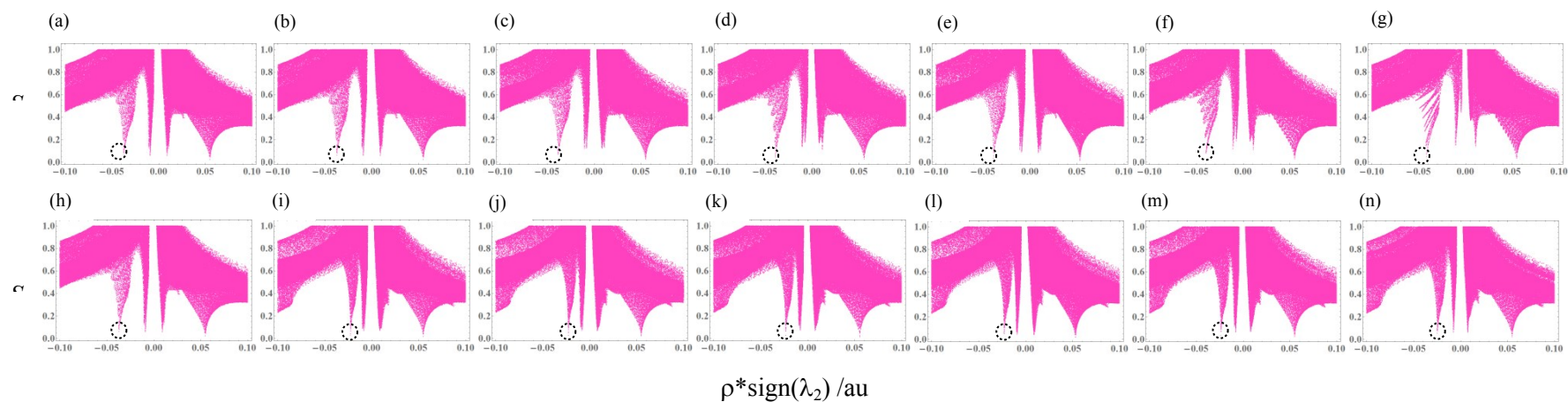


Figure S41: 3D NCI plots. The Gradient isosurfaces ($S=0.20$ au) for (a) AMP–Me₂O, (b) CRL–Me₂O, (c) PHE–Me₂O, (d) FLP–Me₂O, (e) *s*-NPH–Me₂O, (f) CLP–Me₂O, (g) CNP–Me₂O, (h) AMP–Me₂S, (i) CRL–Me₂S, (j) PHE–Me₂S, (k) FLP–Me₂S, (l) *s*-NPH–Me₂S, (m) CLP–Me₂S, and (n) CNP–Me₂S. The data was obtained by evaluating cp-MP2/aug-cc-pVDZ density.

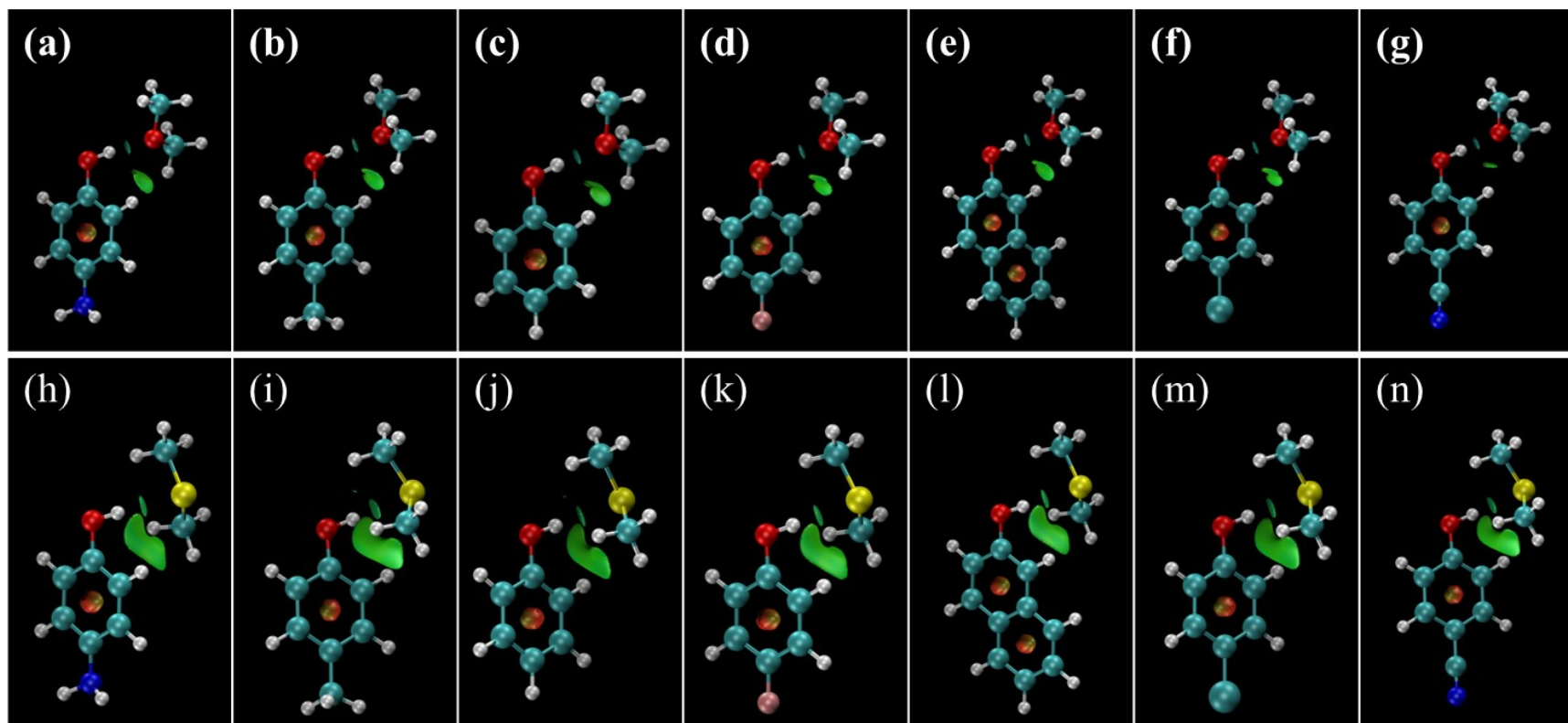


Figure S42: Interacting donor-acceptor natural bond orbitals of AMP–Me₂O [LP(1) of O to $\sigma^*(\text{O-H})$].

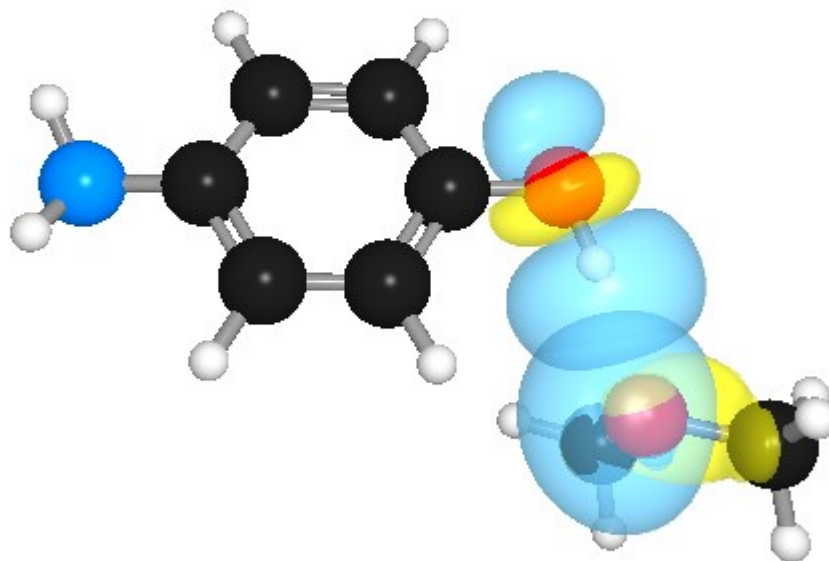


Figure S43: Interacting donor-acceptor natural bond orbitals of AMP–Me₂O [LP(2) of O to $\sigma^*(\text{O-H})$].

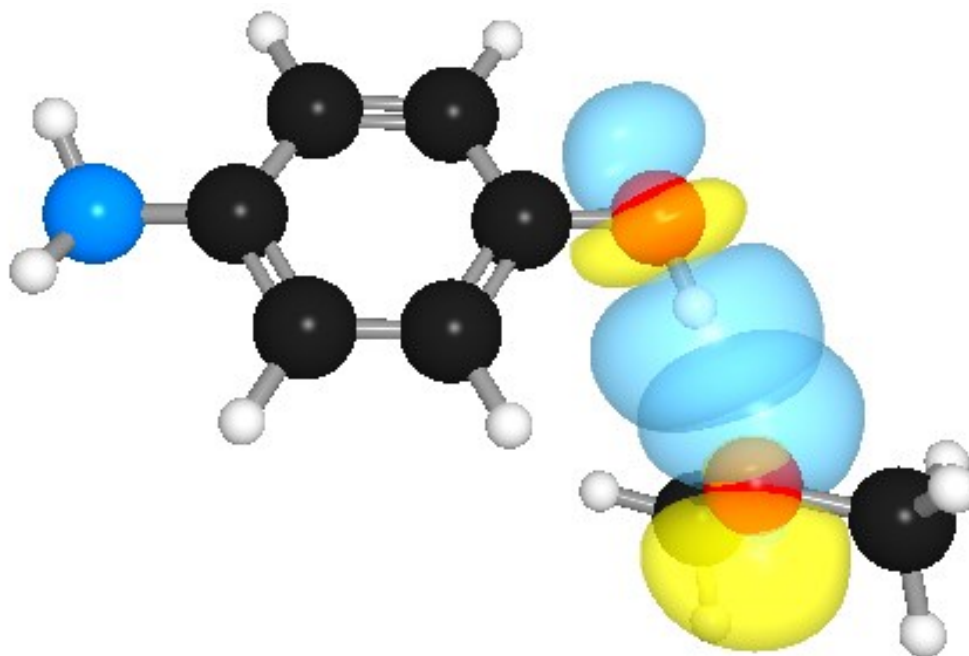


Figure S44: Interacting donor-acceptor natural bond orbitals of AMP-Me₂S [LP(2) of O to $\sigma^*(\text{O-H})$].

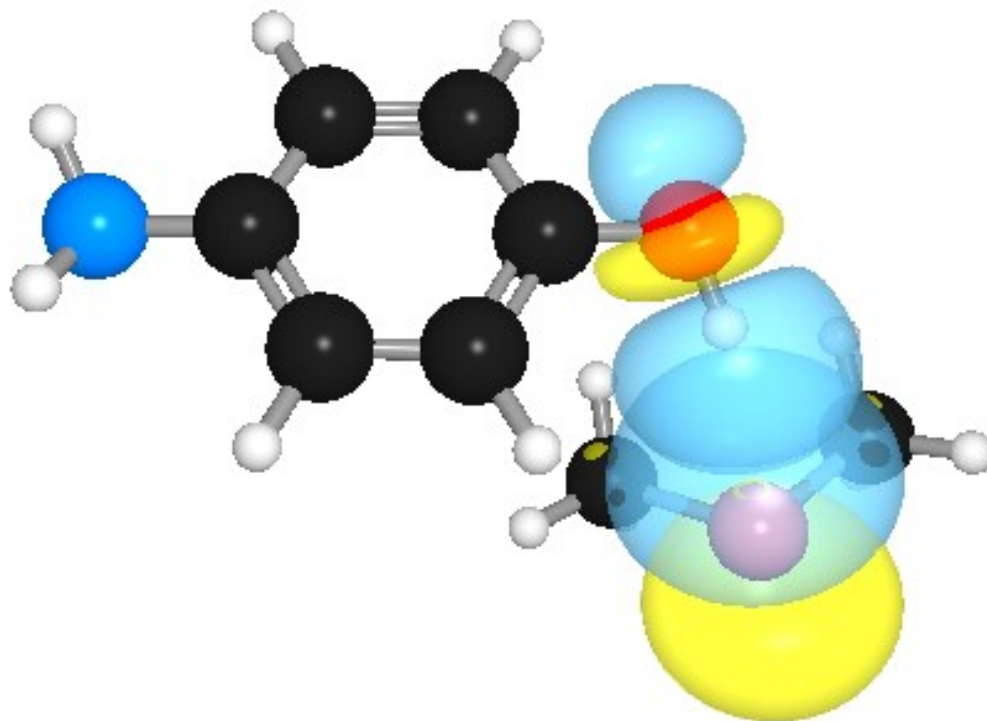


Figure S45 Interacting donor-acceptor natural bond orbitals of CRL–Me₂O [LP(1) of O to $\sigma^*(\text{O-H})$].

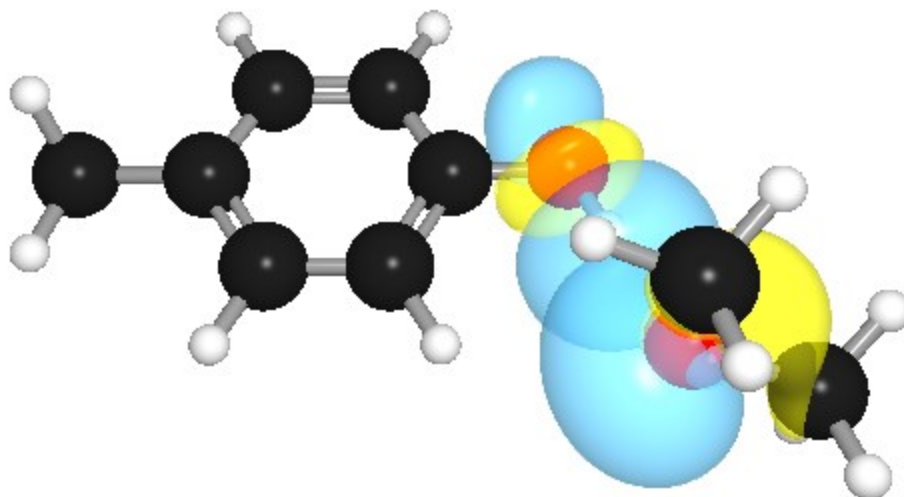


Figure S46: Interacting donor-acceptor natural bond orbitals of CRL–Me₂O [LP(2) of O to $\sigma^*(\text{O-H})$].

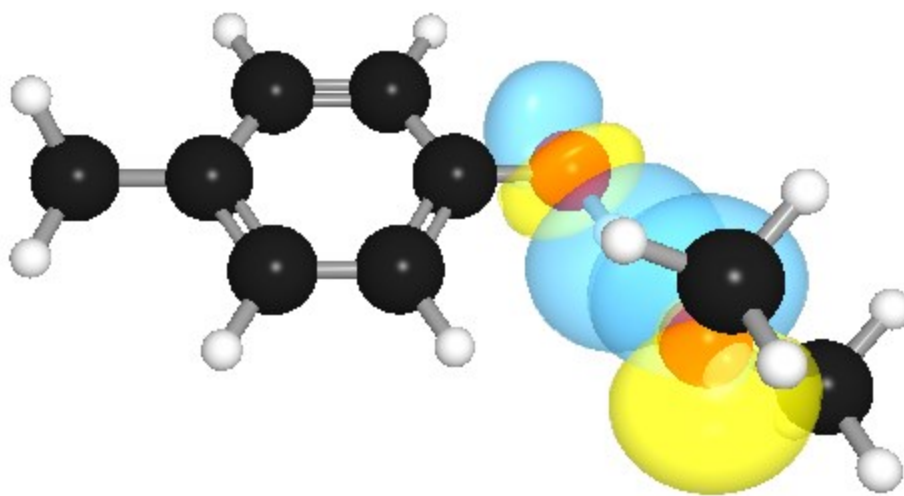


Figure S47: Interacting donor-acceptor natural bond orbitals of CRL–Me₂S [LP(2) of O to $\sigma^*(\text{O-H})$].

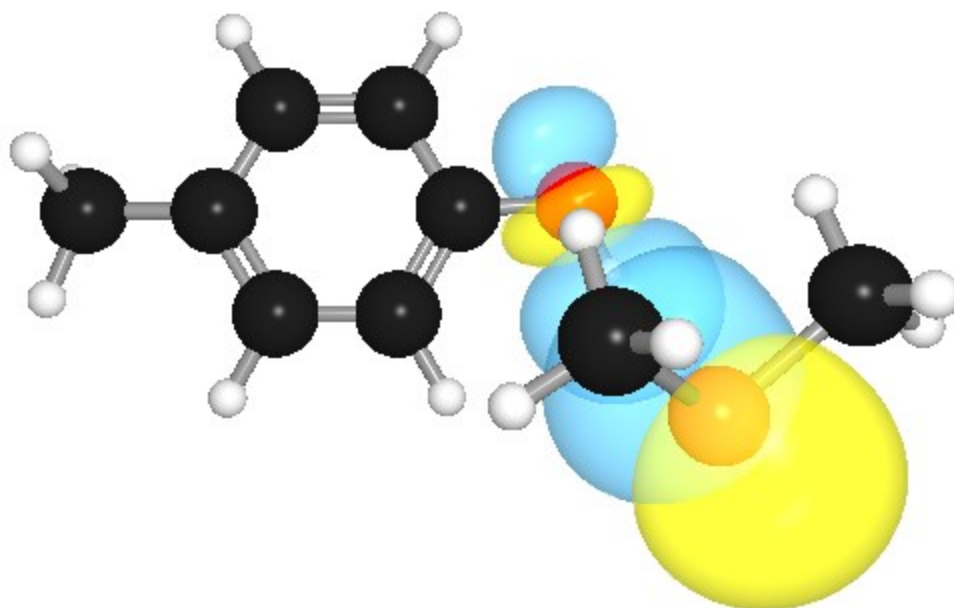


Figure S48: Interacting donor-acceptor natural bond orbitals of PHE–Me₂O [LP(1) of O to $\sigma^*(\text{O-H})$].

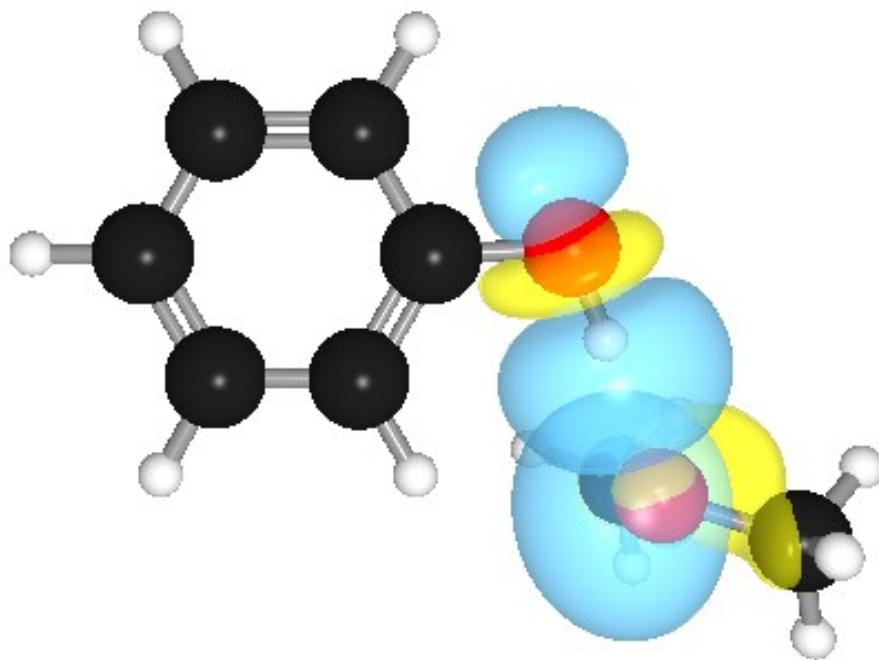


Figure S49: Interacting donor-acceptor natural bond orbitals of PHE–Me₂O [LP(2) of O to $\sigma^*(\text{O-H})$].

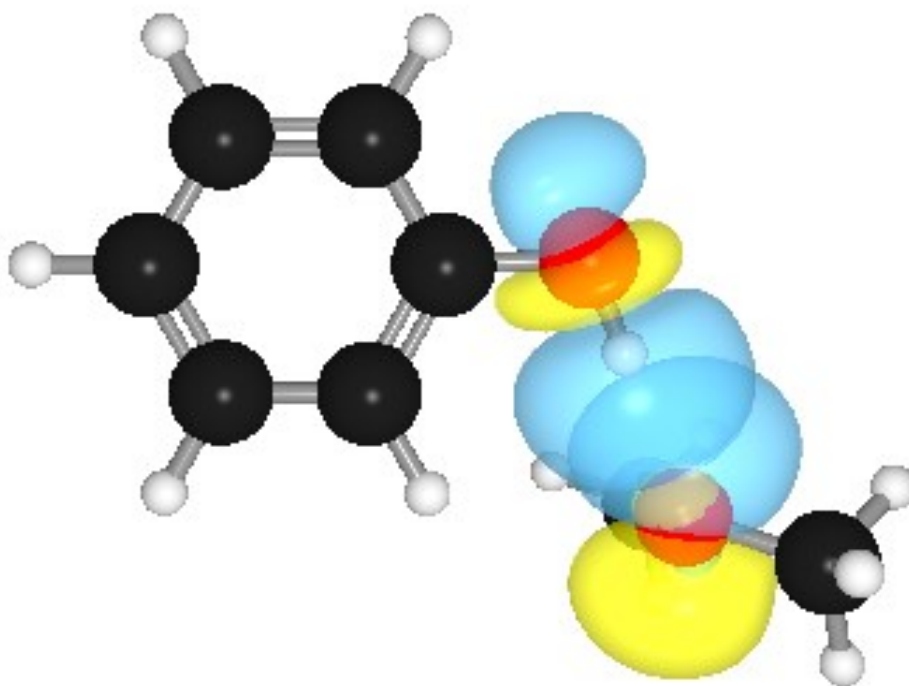


Figure S50: Interacting donor-acceptor natural bond orbitals of PHE–Me₂S [LP(2) of O to $\sigma^*(\text{O-H})$].

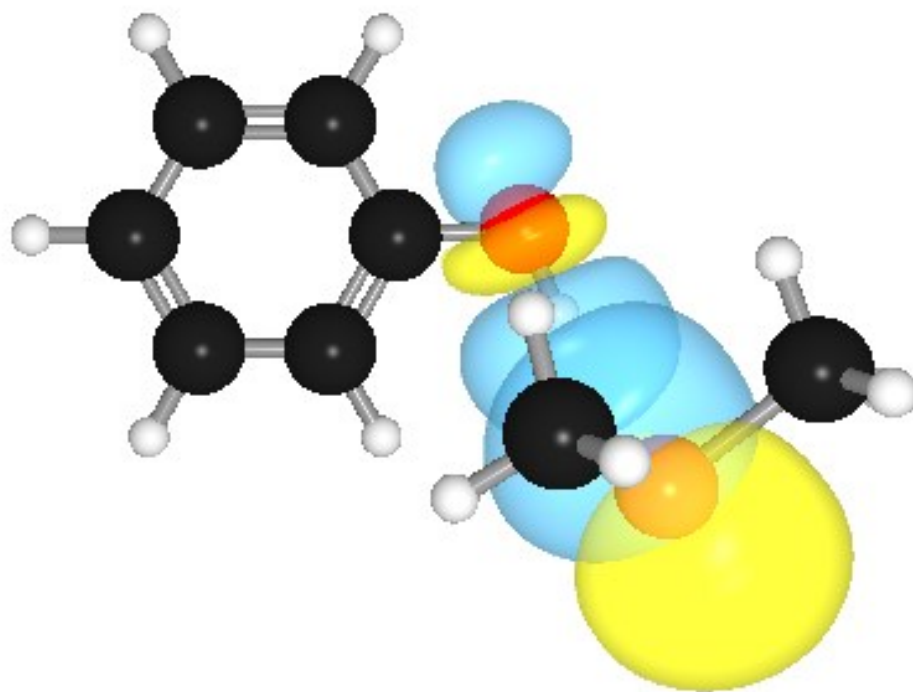


Figure S51: Interacting donor-acceptor natural bond orbitals of FLP–Me₂O [LP(1) of O to $\sigma^*(\text{O-H})$].

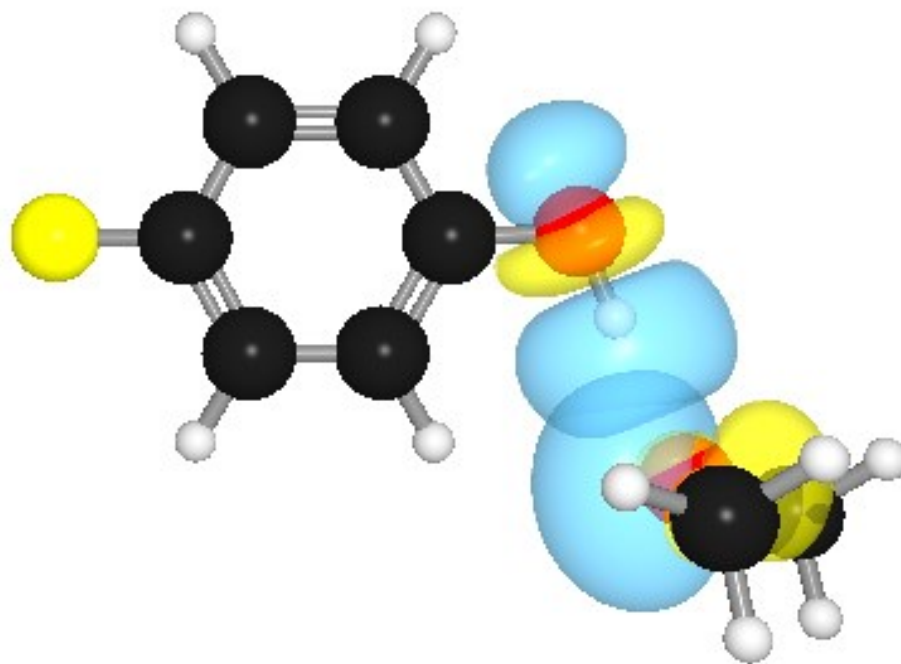


Figure S52: Interacting donor-acceptor natural bond orbitals of FLP–Me₂O [LP(2) of O to $\sigma^*(\text{O-H})$].

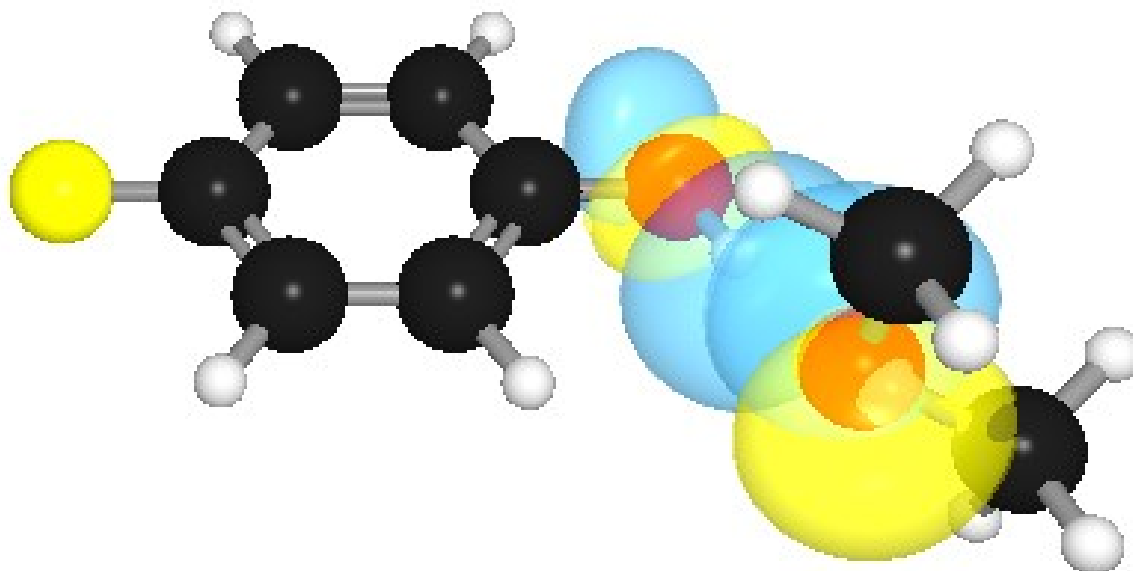


Figure S53: Interacting donor-acceptor natural bond orbitals of FLP–Me₂S [LP(2) of O to $\sigma^*(\text{O-H})$].

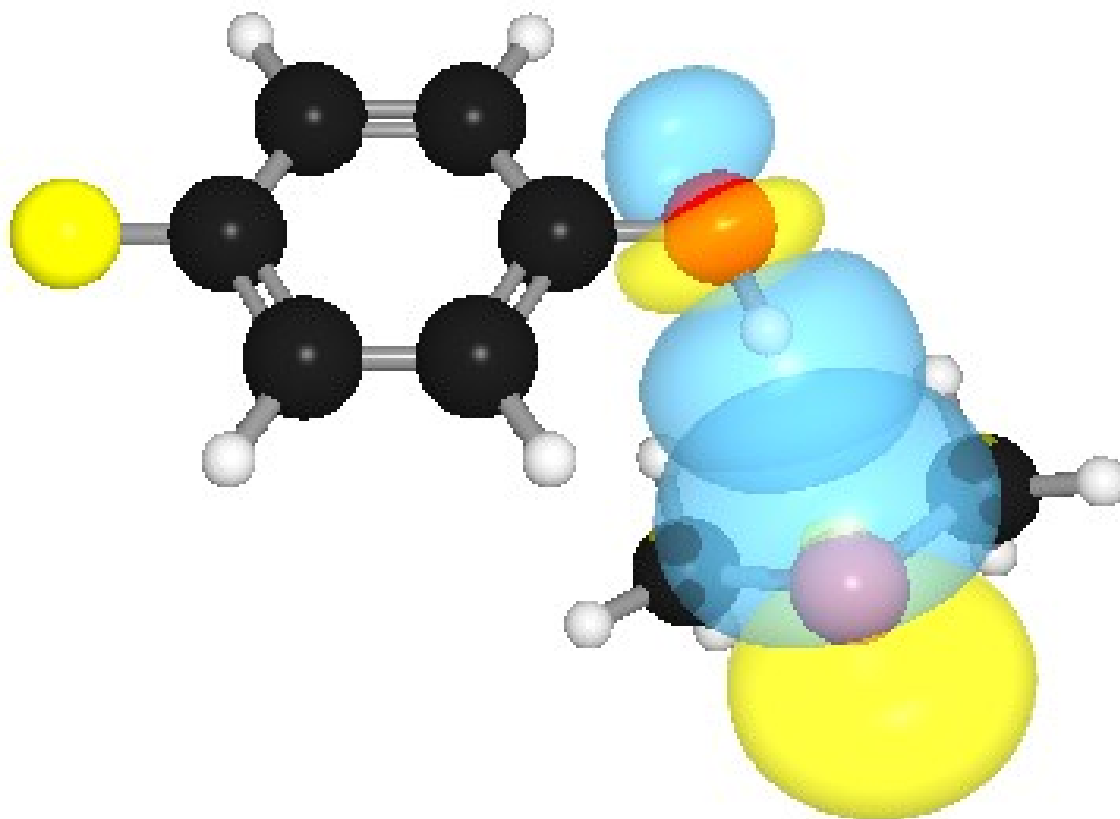


Figure S54: Interacting donor-acceptor natural bond orbitals of *s*-NPH–Me₂O [LP(1) of O to $\sigma^*(\text{O-H})$].

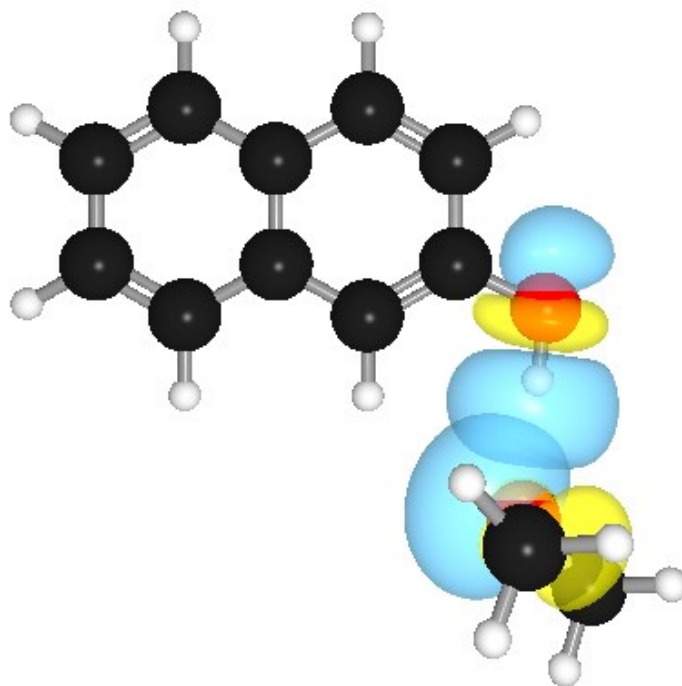


Figure S55: Interacting donor-acceptor natural bond orbitals of *s*-NPH–Me₂O [LP(2) of O to $\sigma^*(\text{O-H})$].

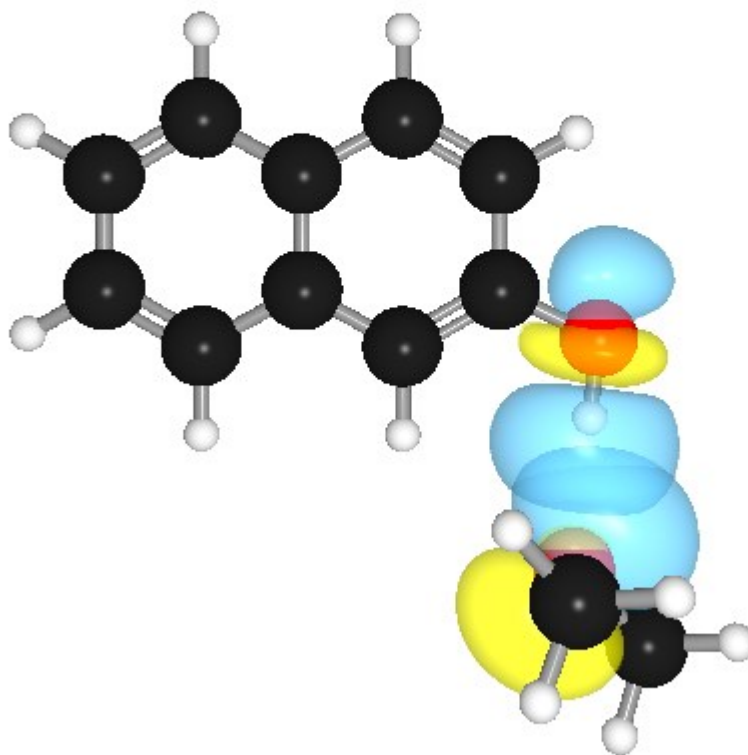


Figure S56: Interacting donor-acceptor natural bond orbitals of *s*-NPH–Me₂S [LP(2) of O to $\sigma^*(\text{O-H})$].

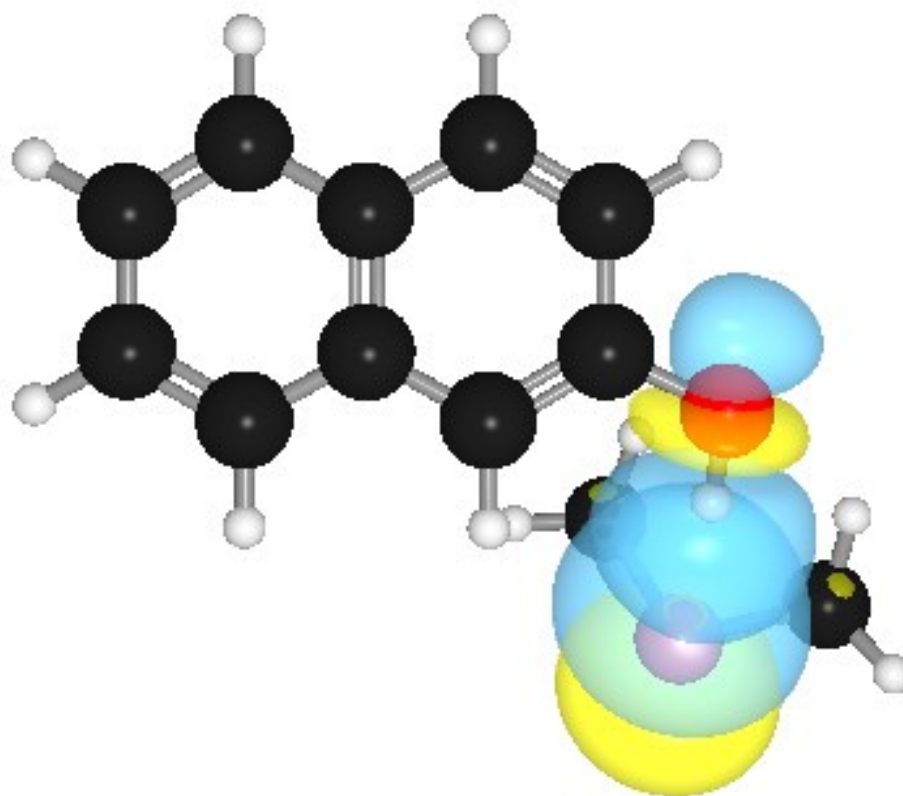


Figure S57: : Interacting donor-acceptor natural bond orbitals of CLP–Me₂O [LP(1) of O to $\sigma^*(\text{O-H})$].

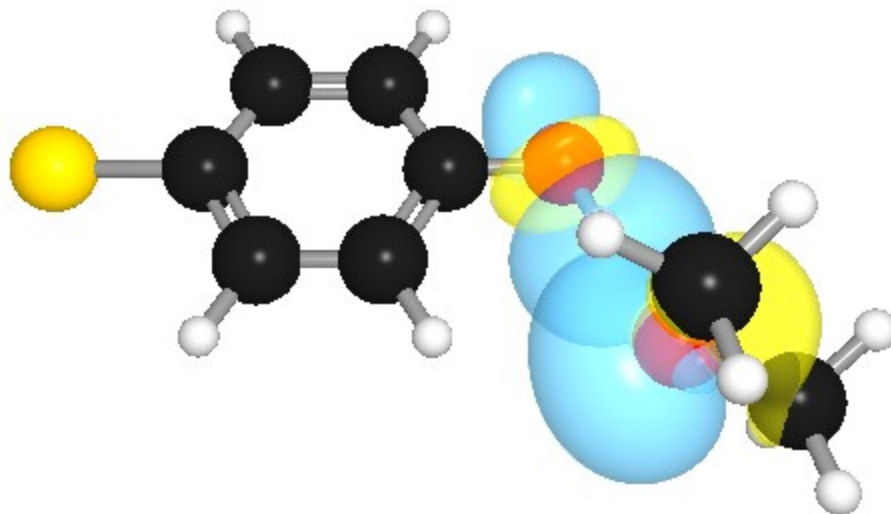


Figure S58: Interacting donor-acceptor natural bond orbitals of CLP–Me₂O [LP(2) of O to $\sigma^*(\text{O-H})$].

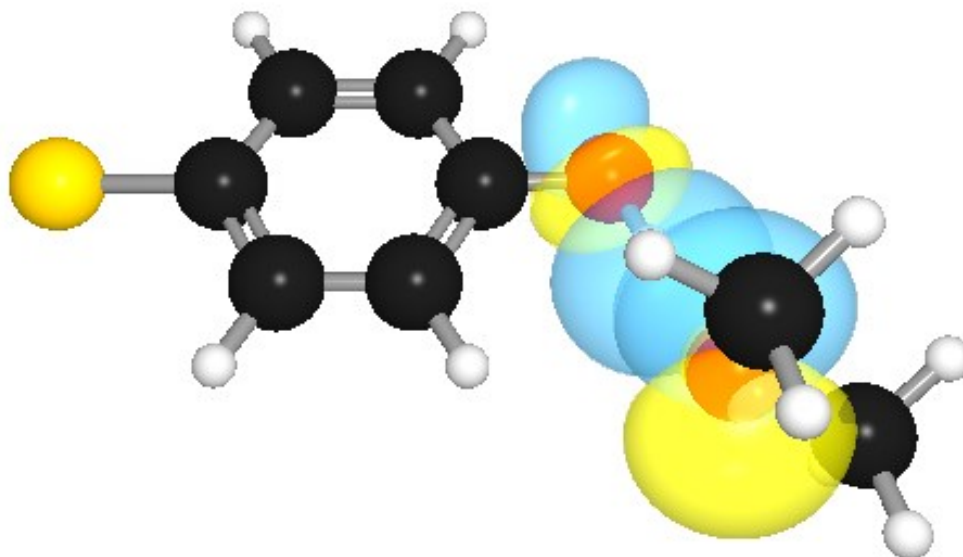


Figure S59: Interacting donor-acceptor natural bond orbitals of CLP–Me₂S [LP(2) of O to $\sigma^*(\text{O-H})$].

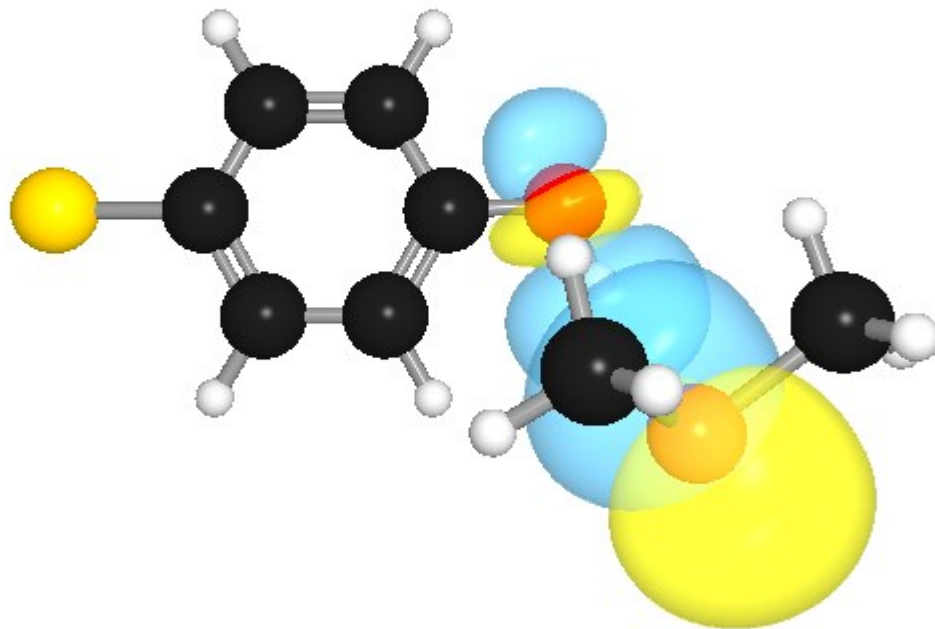


Figure S60: Interacting donor-acceptor natural bond orbitals of CNP–Me₂O [LP(1) of O to $\sigma^*(\text{O-H})$].

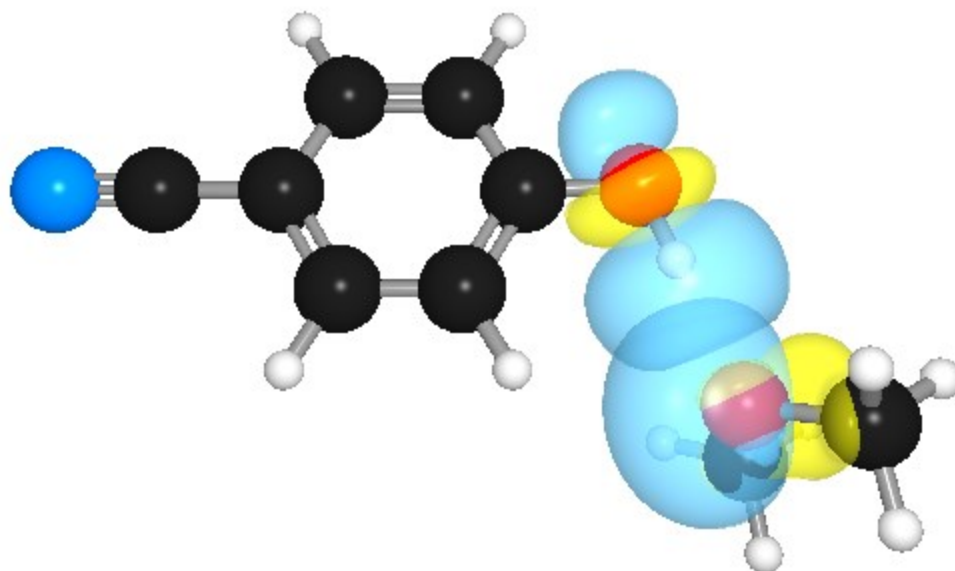


Figure S61: Interacting donor-acceptor natural bond orbitals of CNP–Me₂O [LP(2) of O to $\sigma^*(\text{O-H})$].

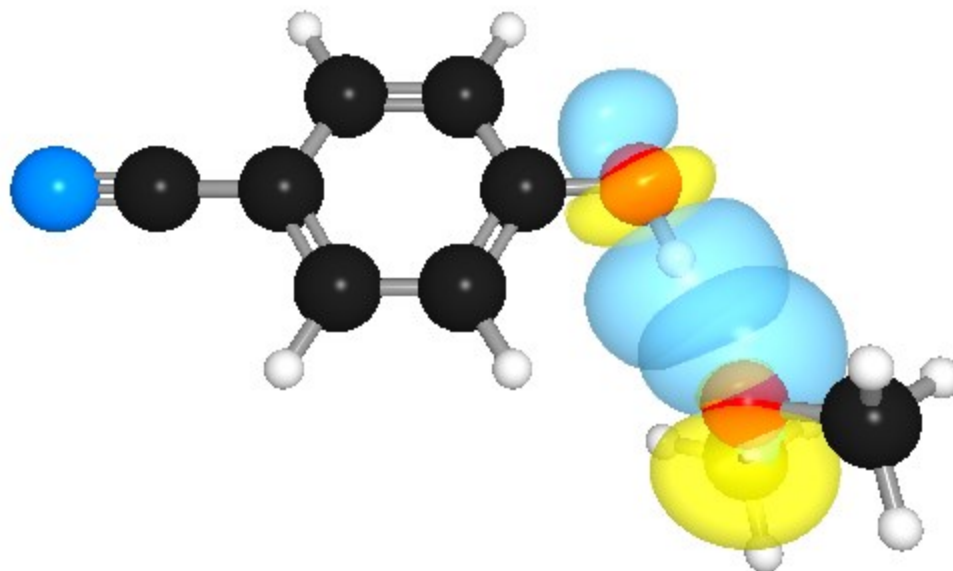


Figure S62: Interacting donor-acceptor natural bond orbitals of CNP–Me₂S [LP(2) of O to $\sigma^*(\text{O-H})$].

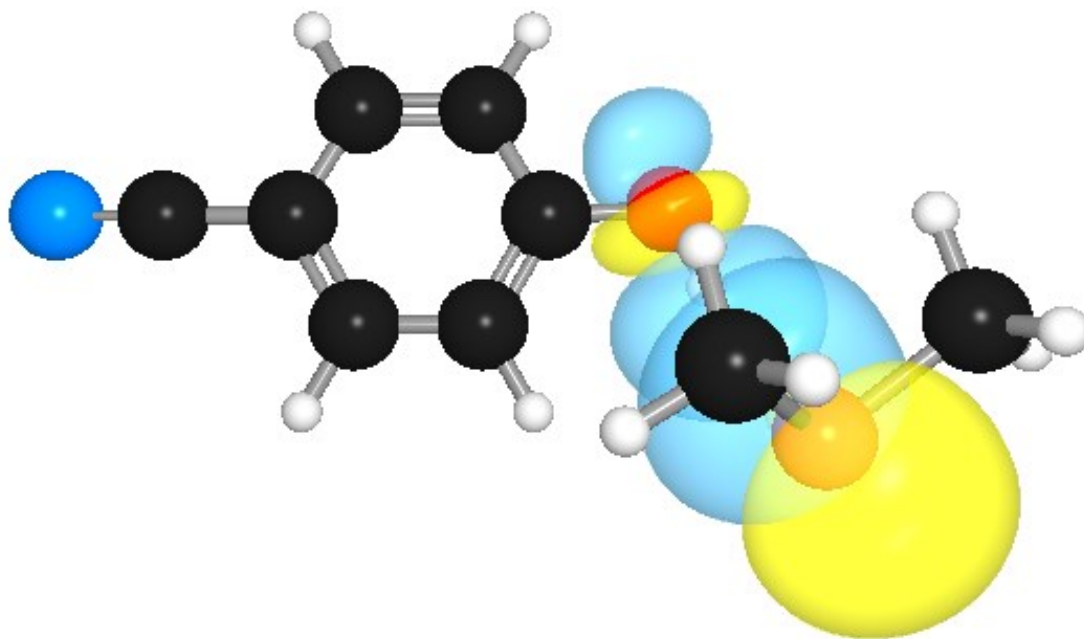


Figure S63: Correlation plots between deprotonation enthalpy and pK_a of H-bond donor phenol derivatives, *p*-aminophenol (AMP), *p*-cresol (CRL), phenol (PHE), *p*-fluorophenol (FLP), β -naphthol (NPH), *p*-chlorophenol (CLP), and *p*-cyanophenol (CNP).

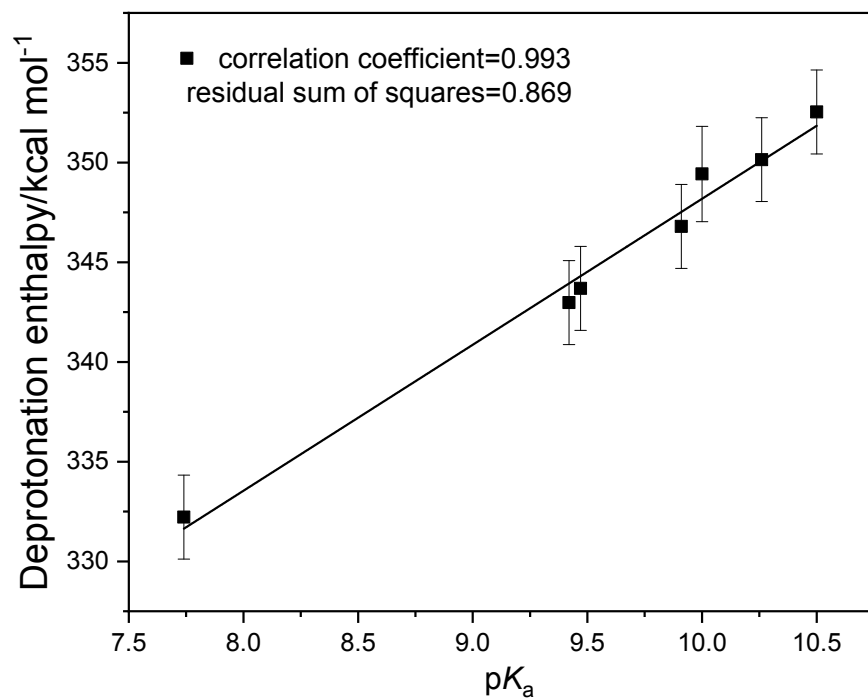


Figure S64: Correlation plots of red shifts in experimentally determined band origin (ΔBO) vs. difference in measured acidity (ΔpK_a) between ground and first electronic excited states for (a) Me_2O (black squares) and (b) Me_2S (red circles) complexes.

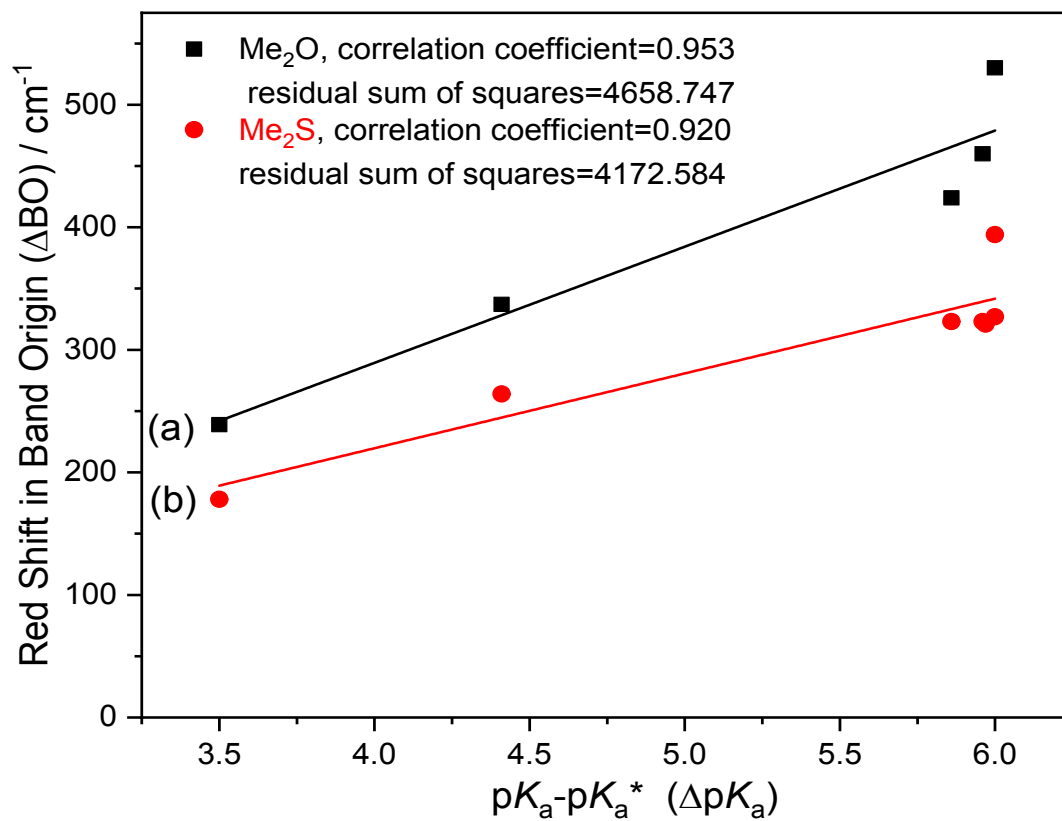


Figure S65: Correlation plots of experimentally determined red shift in O–H stretching frequency ($\Delta\nu_{\text{O-H}}$) vs. computed dissociation energy (D_0 / kcal mol⁻¹) for (a) H₂S (red circles) and (b) H₂O (black squares) complexes.

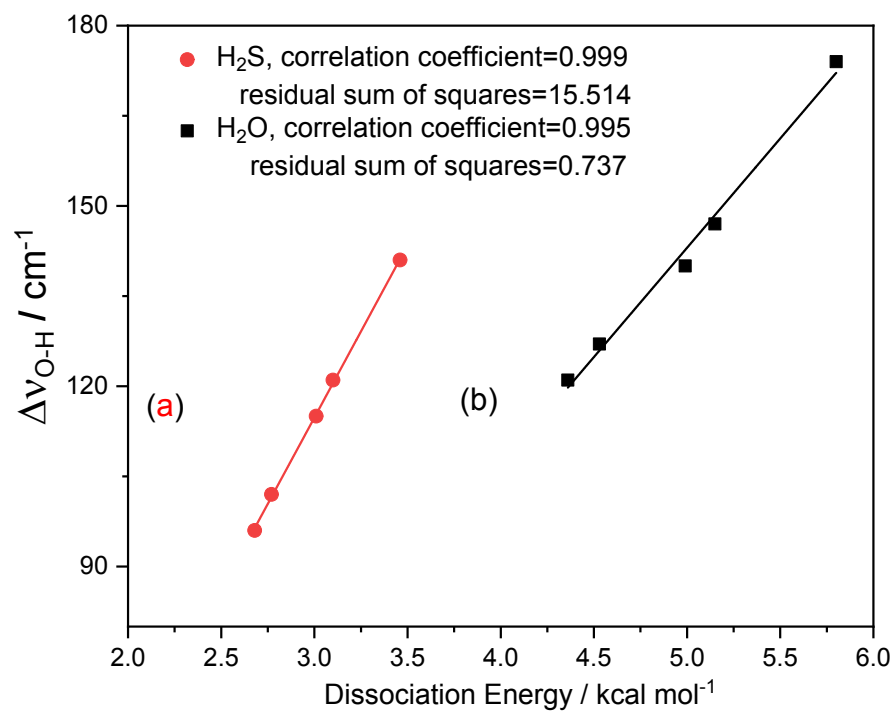


Figure S 66: Correlation plots of red shift in experimentally determined O–H stretching frequency ($\Delta\nu_{\text{O-H}}$) vs. computed E_{ct} for (a) Me_2S (red circles) and (b) Me_2O (black squares) complexes.

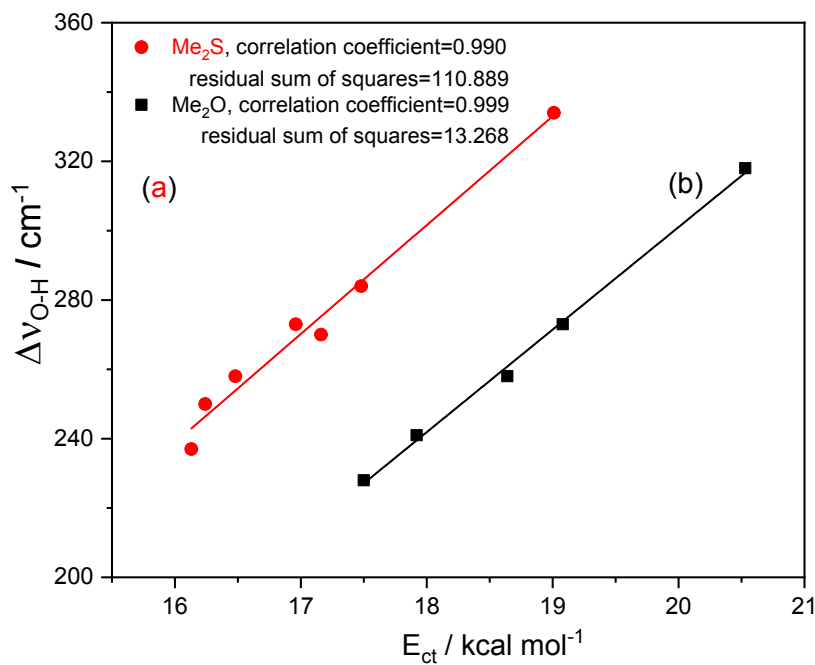


Figure S67: Correlation plots of red shift in experimentally determined O–H stretching frequency ($\Delta\nu_{\text{O-H}}$) vs. computed E_{es} for (a) Me_2S (red circles) and (b) Me_2O (black squares) complexes.

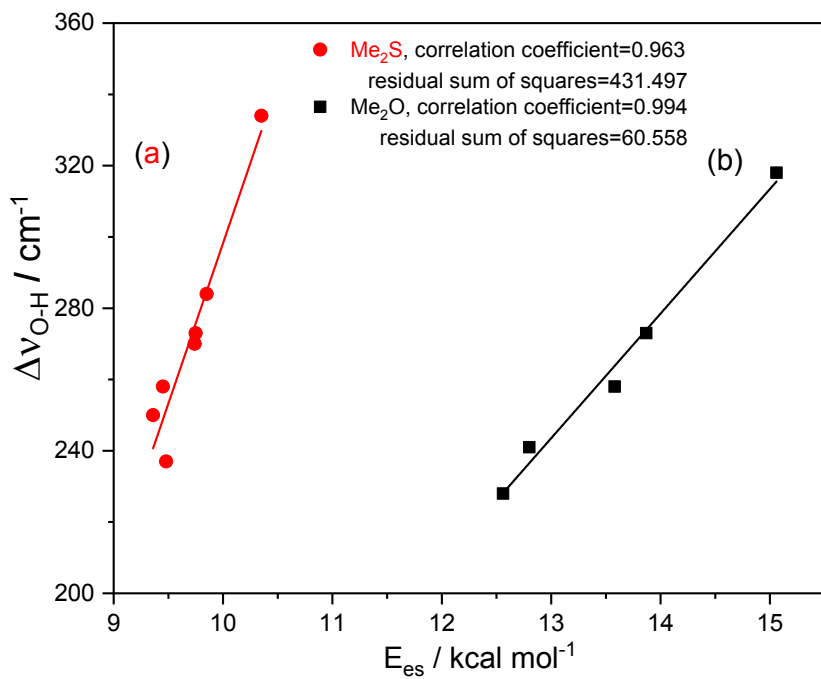
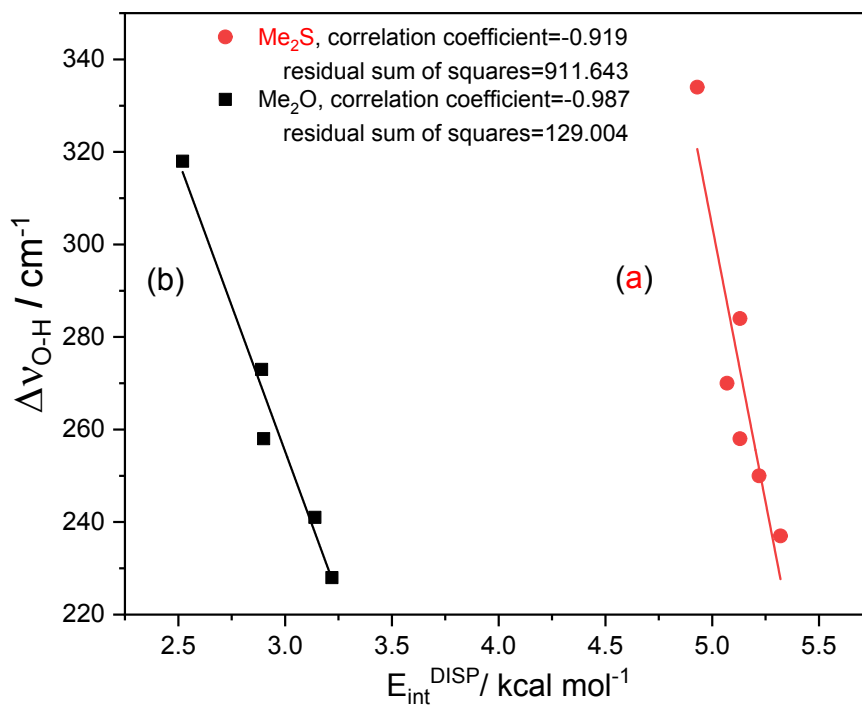


Figure S68: Correlation plots of red shift in experimentally determined O–H stretching frequency ($\Delta\nu_{\text{O-H}}$) vs. computed $E_{\text{int}}^{\text{DISP}}$ for (a) Me_2S (red circles) and (b) Me_2O (black squares) complexes.



Tables

Table S1: List of scaling factors for the phenolic O–H stretching frequency for various substituted phenols and their complexes at different computational methods at aug-cc-pVDZ basis set. Scaling factors were obtained by dividing the experimentally determined O–H stretching frequency of the monomer by that computed one at the respective level of theory.

Methodology	scaling factor						
	AMP	CRL	PHE	FLP	<i>s</i> -NPH	CLP	CNP
cp-MP2	0.9607	0.9608	0.9608	0.9613	0.9619	0.9611	0.9616
MP2	0.9607	0.9608	0.9608	0.9613	0.9619	0.9611	0.9616
cp-B2PLYPD3	0.9560	0.9563	0.9563	0.9569	0.9569	0.9574	0.9572
cp- ω B97X-D	0.9370	0.9373	0.9374	0.9377	0.9370	0.9375	0.9382
cp-LC- ω PBE	0.9374	0.9379	0.9381	0.9388	0.9382	0.9384	0.9392
cp-M06-2X	0.9406	0.9414	0.9422	0.9423	0.9415	0.9417	0.9435
cp-B3LYP	0.9578	0.9582	0.9583	0.9586	0.9584	0.9584	0.9591

+

Table S2: Computed dissociation energies (D_0) and red shifts in IR frequency for various possible conformations of AMP-Me₂A (A=O/S) at MP2 and B3LYP level of theories using aug-cc-pVDZ basis set. The D_0 included the zero point energy (ZPE) contribution and basis set superposition error (BSSE) correction.

conformations (A=O/S)	complexes of Me ₂ O							
	MP2				B3LYP			
	D_0 / kcal mol ⁻¹	$\Delta\nu_0$ / cm ⁻¹			D_0 / kcal mol ⁻¹	$\Delta\nu_0$ / cm ⁻¹		
		O-H	N-H (sym)	N-H (asym)		O-H	N-H (sym)	N-H (asym)
O-H•••A	6.08	280	5	6	4.40	248	7	9
N-H•••A(cis)	3.77	-1	28	13	2.29	-1	40	14
N-H•••A (trans)	3.81	-1	29	13	2.29	-1	41	14
	complexes of Me ₂ S							
O-H•••A	5.57	232	2	3	3.33	249	5	7
N-H•••A (cis)	–	–	–	–	1.02	-1	60	28
N-H•••A (trans)	–	–	–	–	1.21	0	58	27

Table S3: Decomposition of total interaction energies ($E_{\text{int}}^{\text{MP2}}$) by NEDA using cc-pVDZ basis set. This calculation excludes the contribution from zero point energy. $E_{\text{elec}} = \Sigma (E_{\text{es}} + E_{\text{pol}} + E_{\text{se}})$, $E_{\text{int}}^{\text{NEDA}} = \Sigma (E_{\text{elec}} + E_{\text{ct}} + E_{\text{core}})$, $E_{\text{int}}^{\text{DISP}} = (E_{\text{int}}^{\text{MP2}} - E_{\text{int}}^{\text{NEDA}})$. Unfilled places are because the NBO software package we installed and linked with Gamess could not compute those. The interaction energy calculation in NEDA is performed by at the full basis set, so there is no need of counterpoise correction. The delocalized orbitals are first converted into purely localized orbitals by unitary transformation. Therefore all the localized orbitals are either on the individual atoms or on bonds in the complex. If we consider a complex $A \bullet \bullet B$ comprised of two partners A and B, then the $E_{\text{int}}^{\text{NEDA}}$ can be calculated using following formula $E_{\text{int}}^{\text{NEDA}} = E(\psi_{\text{AB}}) - [E(\psi_{\text{A}}) + E(\psi_{\text{B}})]$; where ψ represents the wavefunction of the species. To calculate the different components, NEDA calculates three intermediate wavefunctions: $\psi_{\text{A}}^{\text{def}}$, $\psi_{\text{B}}^{\text{def}}$, and $\psi_{\text{AB}}^{\text{loc}}$; where $\psi_{\text{A}}^{\text{def}}$, $\psi_{\text{B}}^{\text{def}}$ are from the eigenvectors of the A and B blocks of the NBO Fock matrix. They are basically the perturbed wavefunctions of the individual components in the complex. The $\psi_{\text{AB}}^{\text{loc}}$ is on the other hand is the localized wavefunction of AB where inter-component charge transfer is not permitted. It can be expressed as: $\psi_{\text{AB}}^{\text{loc}} = A(\psi_{\text{A}}^{\text{def}}, \psi_{\text{B}}^{\text{def}})$; where A is antisymmetrizer. The CT component can be obtained using below equation: $E_{\text{ct}} = E(\psi_{\text{AB}}) - E(\psi_{\text{AB}}^{\text{loc}})$. Deformation can be obtained by adding deformation contribution of individual fragments, $E_{\text{def}} = \text{DEF}(A) + \text{DEF}(B)$ where $\text{DEF}(A) = E(\psi_{\text{A}}^{\text{def}}) - E(\psi_{\text{A}})$ and $\text{DEF}(B) = E(\psi_{\text{B}}^{\text{def}}) - E(\psi_{\text{B}})$. The sum of the E_{es} , E_{pol} , and E_{ex} can be obtained by $(E(\psi_{\text{AB}}^{\text{loc}}) - E(\psi_{\text{A}}^{\text{def}}) - E(\psi_{\text{B}}^{\text{def}}))$. Additionally NEDA also used linear response theory to subtract self-energy from the individual centres.

complexes	decomposition of interaction energies / kcal mol ⁻¹					
	E _{elec}	E _{es}	E _{pol}	E _{ct}	E _{core}	E _{int} ^{NEDA}
AMP–Me ₂ O	16.84	12.56	8.60	17.50	-29.68	4.66
CRL–Me ₂ O	17.06	12.80	8.57	17.92	-30.07	4.91
PHE–Me ₂ O	17.32	13.02	8.66	18.20	-30.41	5.11
FLP–Me ₂ O	17.94	13.58	8.79	18.64	-30.88	5.70
<i>s</i> -NPH–Me ₂ O	17.79	13.32	9.00	18.69	-31.28	5.20
CLP–Me ₂ O	18.29	13.87	8.92	19.08	-31.46	5.91
CNP–Me ₂ O	19.64	15.06	9.27	20.53	-33.14	7.03
AMP–Me ₂ S	14.02	9.48	9.01	16.13	-28.68	1.47
CRL–Me ₂ S	13.73	9.36	8.66	16.24	-28.41	1.56
PHE–Me ₂ S	13.78	9.45	8.59	16.48	-28.58	1.68
FLP–Me ₂ S	14.09	9.74	8.62	17.16	-29.32	1.93
<i>s</i> -NPH–Me ₂ S	14.33	9.75	9.09	16.96	-29.71	1.58
CLP–Me ₂ S	14.22	9.85	8.66	17.48	-29.69	2.01
CNP–Me ₂ S	14.65	10.35	8.49	19.01	-31.11	2.55

Table S4: Electron occupancy in the O–H σ^* orbital.

Acid	Monomer	Complex		Δe	Complex		Δe
		Me ₂ O	Me ₂ S	Me ₂ S- Me ₂ O	H ₂ O	H ₂ S	H ₂ S-H ₂ O
AMP	0.00521	0.02660	0.02996	0.00336	0.01856	0.01873	0.00017
FLP	0.00530	0.02866	0.03343	0.00477	0.01973	0.02057	0.00084
CLP	0.00543	0.02949	0.03441	0.00492	0.02028	0.02128	0.00100
CRL	0.00547	0.02758	0.03090	0.00332	0.01918	0.01960	0.00042
CNP	0.00565	0.03226	0.03917	0.00691	0.02196	0.02365	0.00169

Table S5: Cartesian coordinates for optimized AMP–Me₂O at cp-MP2/aug-cc-pVDZ level.

C	0.27254600	0.84877400	-0.15287800
C	0.40606200	-0.51851700	-0.46848500
C	1.66642200	-1.14120800	-0.39388800
C	1.41222200	1.58142300	0.22769000
C	2.66773000	0.95455000	0.29326500
C	2.81333500	-0.41531000	-0.01363900
N	4.06922700	-1.06245400	0.13248300
H	-0.47103000	-1.09284600	-0.78441700
H	1.75444000	-2.20653000	-0.63447100
H	1.30394000	2.64267100	0.46832200
H	3.54440900	1.53675200	0.59778000
H	4.85329800	-0.42988600	-0.01148900
H	4.17063100	-1.86359300	-0.48684000
O	-0.93184000	1.51603000	-0.20742300
H	-1.64693700	0.85801500	-0.32943200
O	-2.96645100	-0.43884800	-0.16151800
C	-4.28913000	-0.11270000	-0.60063700
H	-4.21571500	0.17505800	-1.65723900
H	-4.95607800	-0.98720400	-0.49991600
H	-4.70087700	0.72805700	-0.01395900
C	-2.96306100	-0.82481200	1.21933800
H	-3.57916700	-1.72928600	1.36700900
H	-1.92006200	-1.03639800	1.49063000
H	-3.35187200	-0.00829600	1.85358400

Table S6: Cartesian coordinates for optimized CRL–Me₂O at cp-MP2/aug-cc-pVDZ level.

C	-0.26423400	0.84564400	-0.11319100
C	-0.39748300	-0.52495300	-0.41245700
C	-1.66905500	-1.12991000	-0.36599000
C	-1.40747900	1.59782100	0.22196500
C	-2.66719600	0.97893900	0.25861900
C	-2.82290700	-0.39500200	-0.03086300
C	-4.18893600	-1.04534400	0.01744100
H	-4.62988200	-0.97034100	1.02524800
H	-4.88489700	-0.56124000	-0.68741600
H	-4.12655200	-2.11221400	-0.24662300
H	0.48553700	-1.10924700	-0.69193500
H	-1.75935100	-2.19598800	-0.60192900
H	-1.29134900	2.66130500	0.44940300
H	-3.54666700	1.57816300	0.52025700
O	0.94414600	1.50101900	-0.13691600
H	1.65736600	0.84216200	-0.27063200
O	2.98925800	-0.43360600	-0.16357200
C	3.06091800	-0.84845800	1.20673900
H	2.03358400	-1.06169900	1.53133500
H	3.67916600	-1.75851600	1.30099900
H	3.48888400	-0.04735600	1.83536400
C	4.28689600	-0.10376800	-0.67039900
H	4.95317100	-0.98334000	-0.62627400
H	4.15485900	0.20681700	-1.71471700
H	4.73574800	0.72237600	-0.09036100

Table S7: Cartesian coordinates for optimized PHE–Me₂O at cp-MP2/aug-cc-pVDZ level.

C	-0.80560200	-0.63860600	-0.10196300
C	-0.78452000	0.74335000	-0.38606300
C	-1.98194100	1.48260100	-0.34257000
C	-2.02276900	-1.27329900	0.21490200
C	-3.21217500	-0.52593300	0.25100700
C	-3.20027200	0.85545400	-0.02421000
O	0.32632700	-1.41672800	-0.12472100
H	0.16086500	1.22880900	-0.64968900
H	-1.95788400	2.55400500	-0.56493100
H	-2.01772100	-2.34570500	0.42902400
H	-4.15308100	-1.02731900	0.49780300
H	1.10668900	-0.83750300	-0.25410800
H	-4.12794000	1.43341400	0.00624500
O	2.57165100	0.27497600	-0.16004400
C	3.81152300	-0.19078600	-0.70412900
H	3.61790400	-0.47816800	-1.74546500
H	4.57029800	0.61095300	-0.67526700
H	4.18322700	-1.06464200	-0.13975900
C	2.72512300	0.67022300	1.20940700
H	3.44283100	1.50541700	1.29018300
H	1.73690900	0.99424100	1.56246400
H	3.07787400	-0.17750600	1.82333800

Table S8: Cartesian coordinates for optimized FLP–Me₂O at cp-MP2/aug-cc-pVDZ level.

C	-0.32034000	0.82252700	-0.08934100
C	-0.42018500	-0.55936100	-0.35577700
C	-1.67568500	-1.19728000	-0.32450200
C	-1.48138100	1.56578000	0.20113900
C	-2.73817000	0.93677500	0.22990000
C	-2.80944700	-0.43546400	-0.03148400
O	0.87602700	1.49809900	-0.10442400
H	0.47981800	-1.13325700	-0.59746100
H	-1.77379500	-2.26617900	-0.52920000
H	-1.38726000	2.63604400	0.40284000
H	-3.64887800	1.49776000	0.45302500
H	1.60462800	0.85163900	-0.21810100
F	-4.03465500	-1.05342000	-0.00152600
O	2.95117800	-0.38902800	-0.14271100
C	3.13419400	-0.78246500	1.22372800
H	2.13673900	-0.98787400	1.63489500
H	3.75612700	-1.69285100	1.28143500
H	3.61370200	0.02692300	1.80230000
C	4.20390400	-0.07460500	-0.76184800
H	4.86609900	-0.95810000	-0.76074100
H	3.98594400	0.22210800	-1.79569900
H	4.70379000	0.75656600	-0.23336700

Table S9: Cartesian coordinates for optimized *s*-NPH–Me₂O at cp-MP2/aug-cc-pVDZ level.

C	-4.01732500	-1.02533300	0.09357800
C	-3.59907600	0.29810500	0.20573100
C	-2.21973500	0.63890200	0.07613700
C	-1.25431300	-0.40433500	-0.17234100
C	-1.71497200	-1.75153800	-0.28445000
C	-3.06754000	-2.05676800	-0.15403200
C	-1.75653700	1.98619000	0.18209100
C	0.12718200	-0.07090000	-0.30322200
C	0.54342400	1.25495300	-0.18583300
C	-0.40733300	2.28909100	0.05589000
O	1.85343600	1.64993600	-0.29354700
H	-2.48171300	2.78563400	0.36810300
H	-5.07789600	-1.27484600	0.19457200
H	-4.32593900	1.09579600	0.39472000
H	-0.98603100	-2.54676400	-0.47666000
H	-3.40316700	-3.09462500	-0.24293300
H	0.85858000	-0.86063200	-0.50915100
H	-0.04518400	3.31795800	0.13863700
H	2.42084600	0.85121300	-0.34980700
H	4.66254400	-0.49698700	-1.72459700
H	5.42236400	0.01486200	-0.17445400
H	5.17773600	-1.73489200	-0.52438100
H	4.09955900	-0.20906500	1.84261200
H	2.42458200	-0.84605900	1.66977300
H	3.83190000	-1.95729900	1.49403500
O	3.43845200	-0.65610400	-0.09602900
C	4.75521000	-0.72307200	-0.65465800
C	3.45880200	-0.93445400	1.31046700

Table S10: Cartesian coordinates for optimized CLP–Me₂O at cp-MP2/aug-cc-pVDZ level.

C	-0.16359900	0.93725100	0.07812400
C	0.03413500	-0.43566300	0.33559100
C	1.33115300	-0.98110700	0.31166900
C	0.94534700	1.76167300	-0.19591300
C	2.24258000	1.22372300	-0.21737400
C	2.42488600	-0.14661200	0.03433800
O	-1.40318300	1.52441000	0.08533700
H	-0.82422000	-1.07535800	0.56454600
H	1.49023800	-2.04375000	0.51138300
H	0.77853200	2.82451100	-0.39117400
H	3.10491700	1.86043100	-0.42969700
H	-2.08570400	0.82832300	0.19832400
Cl	4.04473400	-0.82369200	0.00473400
O	-3.34033400	-0.49469200	0.13955500
C	-3.52502200	-0.90903700	-1.22060400
H	-2.52482400	-1.04151500	-1.65445200
H	-4.07764300	-1.86396400	-1.25943400
H	-4.07759200	-0.14158300	-1.79101300
C	-4.59842800	-0.27308500	0.78789700
H	-5.19073300	-1.20461300	0.80614600
H	-4.37895500	0.04519200	1.81497700
H	-5.17267500	0.51449800	0.26841800

Table S11: Cartesian coordinates for optimized CNP–Me₂O at cp-MP2/aug-cc-pVDZ level.

C	-0.01051300	0.89843600	-0.02649000
C	0.18045300	-0.48892500	-0.20625800
C	1.47684100	-1.02569700	-0.20658300
C	1.10505400	1.74316000	0.14762000
C	2.40052400	1.21042700	0.14592500
C	2.59276600	-0.17895400	-0.02984400
H	-0.68648700	-1.14083600	-0.35189900
H	1.62759300	-2.09969400	-0.34621700
H	3.26580500	1.86483500	0.28132100
H	0.93816100	2.81492300	0.28356600
C	3.92491500	-0.73109100	-0.03001700
N	5.02339400	-1.18763200	-0.02963300
O	-1.24674000	1.47968600	-0.01378900
H	-1.93592500	0.78306800	-0.09772400
O	-3.20721700	-0.48707000	-0.10201000
C	-4.33243700	-0.30138200	-0.97078400
H	-3.93540100	-0.02623700	-1.95617700
H	-4.91244800	-1.23698300	-1.05143900
H	-4.98726200	0.50413500	-0.59435200
C	-3.62728400	-0.84133200	1.22270100
H	-4.18253800	-1.79509200	1.20639400
H	-2.71854500	-0.95227500	1.82900700
H	-4.26696000	-0.05120800	1.65372400

Table S12: Cartesian coordinates for optimized AMP–Me₂S at cp-MP2/aug-cc-pVDZ level.

C	0.50157500	0.90179300	-0.40814400
C	0.77841400	-0.37731400	-0.92929200
C	2.02130900	-0.98801400	-0.67839900
C	1.48254500	1.56604000	0.35021500
C	2.72560600	0.95525900	0.58670500
C	3.01162800	-0.33113100	0.08071700
O	-0.69965400	1.55084600	-0.61980700
N	4.23534600	-0.97730100	0.39285300
H	0.02896400	-0.89250500	-1.53922300
H	2.22101000	-1.98672300	-1.08214900
H	1.26368800	2.56106900	0.74770800
H	3.47867000	1.48155500	1.18331400
H	-1.35573200	0.88289600	-0.90340600
H	4.99667600	-0.32161700	0.55326600
H	4.51696300	-1.65121400	-0.31556600
S	-2.98964900	-0.75768500	-0.33014800
C	-4.02124400	0.59678000	0.32594500
H	-4.67633900	0.94132600	-0.48732500
H	-4.64105900	0.23216400	1.15881000
H	-3.38554900	1.43085800	0.66067600
C	-2.02919900	-1.09217700	1.18494400
H	-2.70171900	-1.42027500	1.99197600
H	-1.31310900	-1.89500600	0.95730700
H	-1.47207300	-0.19264000	1.48929900

Table S13: Cartesian coordinates for optimized CRL–Me₂S at cp-MP2/aug-cc-pVDZ level.

C	-0.50553400	0.88516900	-0.36823500
C	-0.76909000	-0.40931400	-0.85600200
C	-2.03110500	-0.99499100	-0.63509600
C	-1.50973400	1.58729300	0.32585100
C	-2.76453800	0.99083800	0.52981400
C	-3.04817100	-0.31053700	0.05876100
C	-4.40579200	-0.93770300	0.29224700
H	-4.62389200	-1.02328400	1.36956200
H	-5.20635200	-0.33154800	-0.16273800
H	-4.45405700	-1.94668300	-0.14500900
H	0.00267300	-0.94967600	-1.41452900
H	-2.22477900	-2.00226600	-1.01971800
H	-1.29298000	2.59361600	0.69541200
H	-3.53724300	1.54938000	1.06990300
O	0.70642000	1.51697100	-0.54647500
H	1.35550500	0.85241100	-0.85483200
S	3.05634200	-0.73636600	-0.36001400
C	2.13569400	-1.14609600	1.16128200
H	1.45257100	-1.97509300	0.92609900
H	2.83425800	-1.46244600	1.95062100
H	1.54518400	-0.27887800	1.49518800
C	4.04165600	0.64462500	0.31193900
H	4.68983600	0.28666000	1.12583900
H	4.66821800	1.03448200	-0.50331500
H	3.37792000	1.44371100	0.67617200

Table S14: Cartesian coordinates for optimized PHE–Me₂S at cp-MP2/aug-cc-pVDZ level.

C	-3.42443400	-0.71372200	0.22432500
C	-2.37017500	-1.37099400	-0.43580900
C	-1.17470400	-0.68860200	-0.73075700
C	-1.03039300	0.66192200	-0.35186300
C	-2.08233900	1.32772600	0.30609200
C	-3.27417300	0.63853200	0.58863000
H	-2.47632700	-2.41894500	-0.73276800
H	-0.36154300	-1.19497500	-1.26143700
H	-1.95082500	2.37658700	0.58635900
H	-4.08816000	1.16219800	1.09906500
O	0.11381300	1.38414000	-0.60844200
H	0.81463000	0.76109000	-0.89004700
H	-4.35270400	-1.24627800	0.44815200
S	2.68258900	-0.60248800	-0.35942200
C	1.86559900	-0.98806100	1.22606000
H	1.20027300	-0.16271400	1.52336900
H	1.26535900	-1.89797500	1.08104100
H	2.62154900	-1.17135600	2.00451100
C	3.54489700	0.91622400	0.16933900
H	4.25633700	0.68602600	0.97649600
H	4.09710400	1.30490600	-0.69851100
H	2.81671100	1.66998000	0.50595700

Table S15: Cartesian coordinates for optimized FLP–Me₂S at cp-MP2/aug-cc-pVDZ level.

C	0.55550600	0.85907300	-0.36254300
C	0.79752200	-0.44720900	-0.83511700
C	2.04621100	-1.05956000	-0.61285400
C	1.56864000	1.55905600	0.32056700
C	2.82071700	0.95797700	0.53822200
C	3.03240500	-0.34327600	0.07045300
O	-0.64578400	1.50610500	-0.55096200
H	0.01730300	-0.98203100	-1.38579500
H	2.25445700	-2.07048500	-0.97152200
H	1.36571300	2.57287800	0.67560600
H	3.61987700	1.48518600	1.06468700
F	4.25079000	-0.93432300	0.28604400
H	-1.31069800	0.84471000	-0.83361100
S	-3.01473100	-0.71364300	-0.35926700
C	-4.03261000	0.67215000	0.25158800
H	-4.62652300	1.04696700	-0.59450700
H	-4.71208800	0.32228700	1.04305200
H	-3.38867200	1.48002800	0.63156200
C	-2.14960100	-1.09430500	1.20177200
H	-2.87588300	-1.39836200	1.97050500
H	-1.45762100	-1.92647100	1.00686800
H	-1.57375600	-0.21978400	1.54220600

Table S16: Cartesian coordinates for optimized *s*-NPH–Me₂S at cp-MP2/aug-cc-pVDZ level.

C	4.26266700	-0.88016100	0.33581600
C	3.74168000	0.39335100	0.54927400
C	2.38996500	0.69312400	0.20490000
C	1.56200800	-0.33969300	-0.36908800
C	2.12611100	-1.63491500	-0.57843300
C	3.44868300	-1.90064700	-0.23273300
C	1.82444600	1.98937400	0.40737700
C	0.20945500	-0.04542100	-0.71579700
C	-0.31181400	1.22704400	-0.48880500
C	0.50267700	2.25250800	0.07176400
O	-1.61021400	1.57516000	-0.78350000
H	2.44716300	2.78065200	0.83815200
H	5.30074400	-1.09866800	0.60380200
H	4.36478600	1.18219300	0.98475100
H	1.50228800	-2.42083000	-1.01876400
H	3.86570400	-2.89847800	-0.39983000
H	-0.41439100	-0.82386200	-1.16994300
H	0.06140500	3.24104800	0.22868900
H	-2.11186800	0.75433800	-0.97025500
H	-1.66515600	-1.68819000	1.27441900
H	-2.15260900	0.01194600	1.55950200
H	-3.17084200	-1.34354200	2.18876900
H	-4.28811100	1.12810000	0.46107300
H	-5.39927300	0.26127700	-0.65131900
H	-5.32908000	-0.21326300	1.07610400
S	-3.44275800	-1.05511000	-0.21041100
C	-2.52335400	-1.00645800	1.36519700
C	-4.74001000	0.15318800	0.22209900

Table S17: Cartesian coordinates for optimized CLP–Me₂S at cp-MP2/aug-cc-pVDZ level.

C	-0.08710900	0.98376800	-0.35288800
C	-0.40043900	-0.28897500	-0.87231700
C	-1.68915200	-0.82655500	-0.69845100
C	-1.07257400	1.72341500	0.32865300
C	-2.36329900	1.19572200	0.49807400
C	-2.65985800	-0.07931800	-0.01305600
O	1.15514800	1.55713000	-0.49045100
H	0.35751200	-0.85616000	-1.42233400
H	-1.93863300	-1.81219700	-1.09917800
H	-0.81704100	2.71138400	0.72142000
H	-3.13187800	1.76579000	1.02563900
H	1.78216800	0.86773000	-0.79408600
Cl	-4.26906700	-0.74453600	0.20356200
S	3.38538300	-0.79968400	-0.36998900
C	2.47561700	-1.21266700	1.15714700
H	1.74597900	-1.99770900	0.91076800
H	3.17263100	-1.59171800	1.91961700
H	1.93928000	-0.32798700	1.53399200
C	4.46350400	0.49811900	0.32531900
H	5.10880200	0.07364700	1.10881300
H	5.09176400	0.88151900	-0.49160700
H	3.85610200	1.31965200	0.73495300

Table S18: Cartesian coordinates for optimized CNP–Me₂S at cp-MP2/aug-cc-pVDZ level.

C	-0.24376700	0.95206800	-0.31135000
C	-0.54125900	-0.33861700	-0.79814400
C	-1.83232900	-0.86685100	-0.64547100
C	-1.24839500	1.71653400	0.31550000
C	-2.53993300	1.19459800	0.46406300
C	-2.83660500	-0.10292900	-0.01206300
O	0.99739200	1.51894300	-0.42705100
H	0.23379700	-0.92144700	-1.30573700
H	-2.06645400	-1.86627200	-1.02216300
H	-1.00040400	2.71662600	0.68072600
H	-3.32056900	1.78549500	0.95049000
H	1.63262700	0.83218500	-0.72615700
C	-4.16369500	-0.64507300	0.14546700
N	-5.25756600	-1.09348900	0.27701800
S	3.27164700	-0.77795300	-0.39433400
C	2.44591400	-1.24568400	1.16460900
H	1.72264200	-2.04176500	0.93519100
H	3.18678500	-1.62700200	1.88314100
H	1.91082400	-0.38220900	1.58945500
C	4.36288100	0.52099800	0.27827500
H	5.05444600	0.08731300	1.01575000
H	4.94149800	0.93535700	-0.55983600
H	3.76540700	1.32158900	0.74044500

Sample input file for an anharmonic frequency calculation for a few select modes.

```
%chk=flp_me2o_anharm_OH_str
#MP2/aug-cc-pVDZ opt freq=(anharmonic,selAnharmonicModes) scf=tight
counterpoise=2
```

2-dim anharmonic-frequency computation of flp-me2o complex;
optimization is done using counterpoise correction option; only the OH
stretch and the intermolecular stretch is selected for anharmonic
frequency calculation

```
0 1
C      -0.169635      0.976958      -0.043601      1
C      -0.477187     -0.335310       0.373451      1
C      -1.802388     -0.807760       0.303819      1
C      -1.193192       1.817727     -0.523438      1
C      -2.518647       1.354563     -0.591666      1
C      -2.796276       0.047497     -0.178229      1
O       1.103520       1.491888       0.000262      1
H       0.315362     -0.982665       0.761487      1
H      -2.060842     -1.820343       0.623107      1
H      -0.938733       2.832546     -0.840298      1
H      -3.324907       1.992984     -0.960774      1
H       1.726366       0.778220       0.254028      1
F      -4.088932     -0.408998     -0.246169      1
O       2.891490     -0.624018       0.443678      2
C       4.128273     -0.398602       1.129986      2
H       3.880464       0.052950       2.099050      2
H       4.659068     -1.353445       1.290006      2
H       4.775791       0.286657       0.554512      2
C       3.115104     -1.207767     -0.846563      2
H       3.606827     -2.190890     -0.743500      2
H       2.130711     -1.332820     -1.317213      2
H       3.742670     -0.547105     -1.470637      2
```

```
6 60
```